

27

Subsonic flight

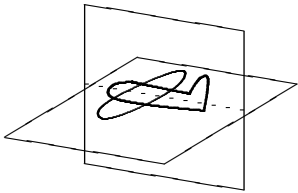
The takeoff of a large airplane never ceases to wonder passengers and bystanders alike. After building up speed during a brief half-minute run, gravity lets go and the plane marvellously lifts off. For this to happen, it is obvious that the engines and the airflow must together generate a vertical force which is larger than the weight of the aircraft. After becoming airborne the airplane accelerates further for a while, and then goes into a fairly steep steady climb until it levels off at its cruising altitude. Aloft in level flight at constant speed, the aerodynamic lift must nearly balance the weight, whereas the engine thrust almost entirely goes to oppose the drag. What is not obvious to most passengers is how the lift depends on the forward speed, the angle of attack, and the shape of the airframe, especially the wings.

The general explanation of aerodynamic lift is quite simple, even if it was only in the beginning of the twentieth century — about the same time as the first generation of airplanes were built — that the details became understood. In nearly ideal flow, pressure is the dominant stress acting on any surface. Consequently, for a lift to exist, the pressure must be higher underneath the wing than above. Bernoulli's theorem then implies that the airspeed must be higher above the wing than below, effectively creating a circulation around the wing, a kind of bound vortex superimposed on the general airflow. Without this circulation, caused by the shape and flying attitude of the wing, there can be no lift.

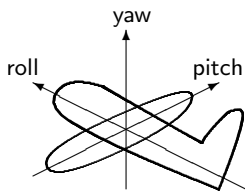
In this chapter we shall only study the most basic theory for subsonic flight with emphasis on concepts and estimates. Aerodynamics is a huge subject (see for example [53, 56]) of importance for all objects moving through the air, such as rifle bullets, rockets, airplanes, cars, birds and sailing ships, and to some extent for submarines moving through water. The potential for triumphant rise and tragic fall unavoidably associated with flying machines makes aerodynamics different from most other branches of science.

27.1 Aircraft controls

Historically aircraft design went through many phases with sometimes weird shapes emerging, especially during the 19'th century. In the 20'th century, where sustained powered flight was finally attained, most of the design problems were solved through systematic application of theory and experiment. The history of the evolution of aerodynamics, the courageous men and their wonderful flying machines, is dramatic to say the least (see for example [54]).



The symmetry plane and wing plane of normal winged aircraft.



The three axes of a normal winged airplane. The aircraft rolls around the longitudinal axis, pitches around the lateral axis, and yaws around the directional axis. The nose lies at the end of the longitudinal axis and the wings in the plane of the longitudinal and lateral axes.

Control surfaces

The majority of all winged aircraft that have ever been built are symmetric under reflection in a midplane. The wings are typically placed in a plane orthogonal to the midplane, but often swept somewhat backwards and a bit upwards. On the wings, and also on the horizontal and vertical stabilizing wing-like surfaces found at the tail-end of most aircraft, there are smaller movable *control surfaces*, connected physically or electronically to the “stick” and the “pedals” in the cockpit. Normally, there are even smaller movable sections of the control surfaces, allowing the pilot to *trim* the aircraft. When the aircraft is trimmed for steady flight, the cockpit controls are relaxed and do not require constant application of force to keep the airplane steady. At cruising speed the aircraft is typically handled with quite small movements of the controls, often carried out by the autopilot, whereas at low speeds, for example during takeoff and landing, much larger moves are necessary.

Main aircraft axes

The symmetry plane and the wing plane of normal aircraft define three orthogonal axes. The first is the *longitudinal* axis, running along the body of the aircraft in the intersection of the midplane and the wing plane. Rotation around this axis is called *roll*, and is controlled by the *ailerons* usually found at the trailing edge of the wings near the wing tips. When the pilot moves the stick from side to side the ailerons move oppositely to each other and create a rolling moment around the longitudinal axis. The second is the *lateral* axis which lies in the wing plane and is orthogonal to the midplane. Rotation around this axis is called *pitch* and is normally controlled by the *elevator*, usually found in the tail of the aircraft. The pilot moves the stick forward and backward to create a pitching moment around the lateral axis. The third is the *directional* axis which is orthogonal to both the wings and the body, and thus vertical in straight level flight. Rotation around this axis is called *yaw* and normally controlled by the *rudder*, also placed in the tail end. In conventional aircraft, the pilot presses foot pedals to move the rudder and create a yawing moment around the directional axis. It was the Wright brothers who first introduced controls for all three axes of their aircraft [54, p. 243].

Wilbur and Orville Wright (1867–1912, 1871–1948). American flight pioneers. From their bicycle shop in Dayton, Ohio, the inseparable brothers carried out systematic empirical investigations of the conditions for flight, beginning in 1896. Built gliders and airfoil models, wind tunnels, engines, and propellers. They finally succeeded in performing the first heavier-than-air, manned, powered flight on December 17, 1903, at Kitty Hawk, North Carolina.

Takeoff, cruise and landing

The takeoff of a normal passenger aircraft begins with a *run* typically lasting half a minute. In modern aircraft with nose wheel, the body stays horizontal during the whole run, whereas in older aircraft with tail wheel or slider, the tail would lift up well into the run and first then make the body nearly horizontal. Having reached sufficient speed for flight, about 250 – 300 km/h for large passenger jet planes, the pilot gently pulls the stick back and thereby raises the elevator, creating a pitching moment that lifts the nose wheel off the runway while the main undercarriage stays in contact with it. After a bit of acceleration in this attitude the undercarriage also leaves the runway, and the aircraft is airborne. For safety reasons the aircraft should not lift off until the speed is somewhat above the minimal speed for flight. In older airplanes, the actual liftoff was almost imperceptible, whereas the powerful engines of modern aircraft make the liftoff much more noticeable through the rather steep climb angle that the aircraft is capable of assuming immediately after. The climb normally lasts until the aircraft has reached cruising altitude, typically 10,000 m, at which point it levels off and accelerates further until it reaches cruising speed, around 800 – 900 km/h for a modern jet. At normal temperature and pressure the sound speed is about 1200 km/h but at cruising altitude the fall in temperature has reduced it by about 10% — as can be seen from (16-8). The airspeed is thus about 85% of sound speed, also called Mach 0.85.

Landing is by far the hardest part of flying. The aircraft has to be brought down to the ground and the speed must be reduced. At low speed the aircraft controls need to be worked harder than at high speed, and random winds and turbulence influence the aircraft much more. Keeping the air speed above stall speed is uppermost in the pilot's mind, because a stall at low altitude makes the airplane crash into the ground. Landing speeds are comparable to takeoff speeds, but the aircraft has to be maneuvered into the narrow space that the runway presents, and in all kinds of weather. Landing lengths can be made shorter than takeoff lengths by diverting jet exhaust into the forward direction or reversing propeller blades, in addition to application of wheel brakes.

Example 27.1.1: Jet engines develop nearly constant thrust (force) at a given altitude such that their power (energy output per unit of time) increases proportionally with airspeed, all other factors being equal. Propeller engines yield instead roughly constant power so that the thrust decreases with airspeed. Ignoring air resistance (drag), the constant thrust from jet engines translates into nearly constant acceleration during the takeoff run. A typical large passenger jet airliner (Boeing 747-200) has a maximal weight of 374,000 kg and four engines that together yield a maximum thrust of 973,000 N, corresponding to a runway acceleration of 2.6 m/s^2 when fully loaded. At this acceleration the plane reaches takeoff speed of 290 km/h in 31 s after a run of about 1250 m. Actual takeoff length is somewhat larger because of drag and rolling friction. For safety reasons, runways are required to be at least twice that length, typically between 3 and 4 km.

Extreme flying

An aircraft can in principle move through the air in any attitude — and some pilots enjoy making their planes do exactly that — but there is an intended normal flying attitude with the wings nearly horizontal and orthogonal to the airflow. In this attitude, the aircraft is designed such that the flow of over the wings and body of the aircraft is as laminar as possible, because laminar flow yields the largest lift force and smallest drag.

In other attitudes, steep climb, dive, roll, loop, tight turn, spin, tail-glide, sideways crabbing, and what not, the airflow over the wings may become turbulent resulting in almost complete loss of lift. When that happens, the aircraft is said to have *stalled*. Stalling an aircraft in level flight at sufficient altitude is a common – and fun – training exercise. First the engine power is cut to make the aircraft slow down. While the airspeed is falling the pilot slowly pulls back the stick to pitch the nose upwards so that the aircraft keeps constant altitude. This can of course not continue, and at a critical point the laminar flow over the wings is lost and replaced by turbulence. The aircraft suddenly and seemingly by its own volition pitches its nose downwards and begins to pick up speed in a dive. A modern aircraft normally recovers all by itself and goes into a steady glide at a somewhat lower altitude. A stall close to the ground can be catastrophic, as the many hang-glider accidents can confirm (the first fatal one happened in 1896 and cost the life of flight pioneer Otto Lilienthal).

Most aircraft are today equipped with mechanical stall detection devices near the leading edge of the wings, and audible stall warnings are frequently heard in aircraft cockpits during landing, just before touchdown. The warnings indicate that a stall in the wing flow is imminent, although the aircraft will usually not go into a proper stall before touching down.

Other situations may arise in which only a part of the lifting surfaces stall. In a tight turn at low speed, the inner wing may stall whereas the outer wing keeps flying, and the aircraft goes into a vertical *spin*. In the early days of flight it was nearly impossible to recover from such a situation which easily could arise if the aircraft was damaged, for example in air combat. In those days pilots were not equipped with parachutes, and they often saw no other way out than jumping from the airplane, rather than burn with it. Today's passenger aircraft are not cleared for spin, but it can be fun to take a modern small aircraft that *is* cleared for aerobatics into a spin at sufficient altitude, for example by pulling hard back and sideways at the stick just before it otherwise would go into a normal stall, as described above. Most people find the experience quite unpleasant and disorienting, especially due to the weightlessness that is felt while the aircraft slowly tumbles over before it goes into a proper spin. Again, modern aircraft are so stable that they tend to slip out of a spin by themselves if the controls are left free.

Otto Lilienthal (1848–1896). German engineer. One of the great pioneers of manned flight. Over more than two decades he carried out systematic studies of lift and drag for many types of wing surfaces and demonstrated among other things the superiority of cambered airfoils. Constructed (and exported!) manned gliders, and also took out patents on such flyers in 1893. Stalled and crashed from a height of about 17 meters outside Berlin on August 9, 1896. Whether he would actually have invented powered flight before the Wright brothers did in 1903 is not clear [54]

27.2 Aerodynamic forces and moments

There are several stages in the process of getting to understand flight. The first of these concerns the global forces and moments that act on a moving body completely immersed in a nearly ideal fluid such as air. Initially we put no constraints on the shape of the object or on the motion of the air relative to the object, although mostly we shall think of an aircraft under normal flight conditions, and mostly we shall discuss only the forces acting on it and apart from scattered comments leave the discussion of moments to more specialized treatments [53].

Total force

The total force \mathcal{F} acting on a body determines the acceleration of its center of mass. The only way a fluid can act on an immersed body, is through contact forces, described by the stress tensor $\boldsymbol{\sigma} = \{\sigma_{ij}\}$. Including the weight $M\mathbf{g}_0$ and engine thrust \mathbf{T} the total force becomes,

$$\boxed{\mathcal{F} = \mathbf{T} + M\mathbf{g}_0 + \mathcal{R}} . \quad (27-1)$$

where

$$\mathcal{R} = \oint_S \boldsymbol{\sigma} \cdot d\mathbf{S} , \quad (27-2)$$

is the resultant of all contact forces, also called the *reaction force*. In principle this includes hydrostatic buoyancy forces (see chapter 5), which serve to diminish the effective gravitational mass of a body. For heavier-than-air flying, buoyancy can normally be disregarded.

Lift and drag

It is convenient to resolve the reaction force into two components, the *lift* which is orthogonal to the instantaneous center-of-mass velocity \mathbf{U} of the aircraft, and the *drag* which is parallel with it,

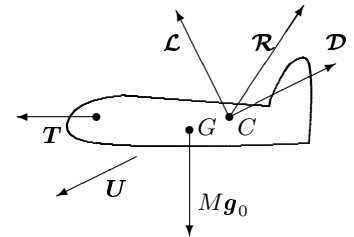
$$\mathcal{R} = \mathcal{L} + \mathcal{D} \quad (27-3)$$

satisfying

$$\mathcal{L} \cdot \mathbf{U} = 0 , \quad \mathcal{D} \times \mathbf{U} = \mathbf{0} . \quad (27-4)$$

The drag is always acts in the opposite direction of the center-of-mass velocity whereas the lift may take any direction orthogonal to it.

Lift may even point directly downwards. It is for this reason dangerous to fly an aircraft inverted on the back close to the ground, because the gut reaction of pulling the stick towards you to get away from the ground will generate an extra lift which sends you directly into the ground. During banked turns an airplane also generates lift away from the vertical, creating in this way the force necessary to change its direction.



Sketch of the forces acting on a body moving with instantaneous center-of-mass velocity \mathbf{U} . The thrust \mathbf{T} propels the object forward, gravity $M\mathbf{g}_0$ pulls it down, and the aerodynamic reaction force \mathcal{R} may be resolved into lift \mathcal{L} and drag \mathcal{D} . Notice that the reaction \mathcal{R} and its components are plotted as acting in a single point C , called the aerodynamic center, although this concept may not always be meaningful. For stability the center of thrust should lie forward of the aerodynamic center.

* **Total moment of force**

The total moment of all forces acting on the body is

$$\mathcal{M} = \mathcal{M}_T + \mathbf{x}_G \times M\mathbf{g}_0 + \mathcal{M}_R, \quad (27-5)$$

where \mathcal{M}_T is the moment of thrust, \mathbf{x}_G the center of gravity of the body, and the moment of the contact forces is,

$$\mathcal{M}_R = \oint_S \mathbf{x} \times \boldsymbol{\sigma} \cdot d\mathbf{S}. \quad (27-6)$$

The total moment depends on the choice of origin for the coordinate system, but if the total force \mathcal{F} on the body vanishes, the total moment becomes independent of the origin. In that case one may calculate the total moment around any convenient point, for example the center of gravity. The individual contributions to the total moment will depend on the choice of origin, even if their sum is independent.



The two situations above are physically equivalent. In the upper drawing the center-of-mass moves with velocity U to the left. In the lower, the center-of-mass does not move, but the surrounding air moves with velocity U to the right at great distances from the object.

27.3 Steady flight

In steady flight the aircraft moves with constant center-of-mass velocity in a non-accelerated frame of reference, so that the sum of all forces must vanish

$$\mathbf{T} + M\mathbf{g}_0 + \mathcal{L} + \mathcal{D} = \mathbf{0}. \quad (27-7)$$

Even if passenger comfort demands that the pilot tries to achieve nearly vanishing total force on an airplane, irregular motion of the air may buffet the plane around. In extreme cases, unannounced clear air turbulence may suddenly cause unfettered passengers to fly around inside the cabin. We shall disregard such phenomena and assume that the aircraft is capable of flying with a steady velocity through an atmosphere that would have been at rest were it not for the moving aircraft. Since forces in Newtonian mechanics are the same in all inertial reference frames, we shall feel free to work in the rest-frame of the aircraft where the air asymptotically moves at constant speed.

In the same way as floating bodies, ships and icebergs, should be in stable hydrostatic equilibrium, aircraft should also preferably be dynamically stable in steady flight, meaning that a small perturbation of the aircraft's steady, non-rotating flying attitude should generate a moment counteracting the perturbation. In general this requires the center of thrust to lie forward of the aerodynamic center. Most modern aircraft are dynamically stable when properly trimmed, and that is very good for amateur pilots, but in military fighter planes, dynamic stability is sometimes traded for maneuverability. Certain modern fighter planes can in fact only maintain a stable attitude through corrections continually applied to the control surfaces by a fast computer.

The main attitude parameter responsible for lift is the *angle of attack* α , also called the *angle of incidence*, between the airflow and the plane of the aircraft, formed by the longitudinal and lateral axes. In normal flight at high speed the angle of attack is usually quite small, typically a couple of degrees.



The angle of attack α is the angle between airflow U and the plane of the aircraft.

Steady climb

After acceleration and takeoff a powered aircraft normally goes into a steady climb forming a constant positive *climb angle* (or *angle of ascent*) θ with the horizon.

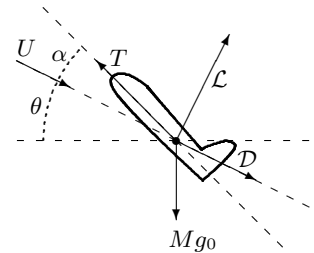
Cockpit instruments usually indicate the *rate of ascent* or *climb rate* $U \tan \theta$ rather than the climb rate. Having reached cruising height the pilot reduces power to a fuel-economic setting and the aircraft levels off with $\theta = 0$ and a tiny angle of attack. Finally, approaching its destination, the aircraft power is reduced, though usually not cut completely off, and the aircraft goes into a powered descent with negative θ . Just before landing, power is lowered to near zero, the aircraft flares out almost horizontally ($\theta \approx 0$) with nose up under a fairly large angle of attack before the final touchdown.

Assuming that the thrust is directed along the longitudinal axis (as is normally the case for fixed-wing aircraft¹), we obtain the following expressions for lift and drag by projecting the forces on the direction of motion and the direction orthogonal to it,

$$D = T \cos \alpha - Mg_0 \sin \theta, \quad L = -T \sin \alpha + Mg_0 \cos \theta. \quad (27-8)$$

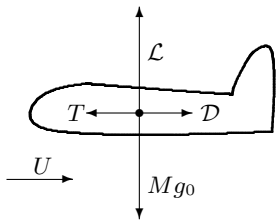
Given the values of all the parameters on the right hand sides, we may calculate the values of lift and drag that are required to keep the aircraft in steady flight.

This is, however, not really the way a pilot operates an aircraft. Typically, the pilot selects a power setting for the engine(s) and a certain rate of climb, and then waits until the aircraft steadies on a certain airspeed, angle of attack, and angle of climb. This procedure of course presupposes that there are such solutions within the aircraft's flight envelope for the specified values of power and climb rate (if not, the aircraft will stall). We shall later see that aerodynamic theory allows us to calculate lift and drag for a given aircraft in terms of the airspeed, the angle of attack, and the air density. The steady flight equations (27-8) may then be solved for the airspeed U and the angle of attack α , given the air density, the weight, the engine power, and the climb rate. There is the further complication that for a given engine setting the thrust T tends to fall inversely with airspeed for propeller engines whereas it stays more or less constant for jets. On top of that, the air temperature, pressure, and density all vary with flying altitude.



Forces acting on an aircraft in powered steady climb at an angle θ with angle of attack α . All the forces are assumed to lie in the symmetry plane of the aircraft. For convenience we have moved all forces to the center of gravity.

¹In other types of aircraft, the engine thrust can also have a component orthogonal to the longitudinal axis. Such a thrust component will contribute to lift, and in the extreme case of a helicopter there is almost no other lift, and the engine thrust balances by itself both drag and weight.



Sketch of forces in steady horizontal powered flight with a small angle of attack. Lift balances the weight and drag balances the thrust.

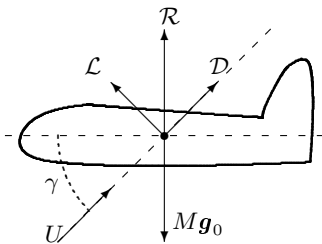
In steady level flight with small angle of attack, $\theta = 0$ and $\alpha \approx 0$, it follows that lift must balance weight and thrust must balance drag. During steady climb with a small angle of attack, $\alpha \ll 1$, the steady flight equations (27-8) may be written

$$\sin \theta \approx \frac{T - \mathcal{D}_0}{Mg_0}, \quad \mathcal{L} \approx Mg_0 \cos \theta, \quad (27-9)$$

where \mathcal{D}_0 is the residual drag at zero angle of attack. Thus, the ratio of the excess of power $T - \mathcal{D}_0$ to the weight of the aircraft Mg_0 determines the climb angle. To get a finite positive angle of climb, the thrust must not only overcome the drag but also part of the weight of the airplane. From climb angle, one can afterwards calculate the lift that the airflow over the wings and body of the aircraft necessarily must generate to obtain a steady climb.

Example 27.3.1: During initial climb, speed is fairly low, and if drag can be ignored relative to thrust it follows that $\sin \theta \lesssim T/Mg_0$. For the fully loaded Boeing 747-200 of example 27.1.1 we find $T/Mg_0 \approx 0.27$ and thus $\theta \lesssim 15^\circ$.

Unpowered steady descent



Sketch of forces in unpowered steady descent at a glide angle γ . Lift and drag collaborate to balance the weight. The airplane can glide with many different angles of attack (here shown with $\alpha = \gamma$) but there is a best angle of attack which yields the smallest glide angle, or equivalently the highest glide ratio.

Most freely falling objects quickly reach a constant terminal velocity. Stones fall vertically, whereas aircraft, paper gliders, paragliders, and parachutists in free fall in addition will attain sometimes large horizontal speeds. An aircraft in unpowered flight is able to glide towards the ground with constant velocity and constant rate of descent. It is part of early training for pilots to learn how to handle their craft in unpowered steady descent, and usually the aircraft is so dynamically stable, that it by itself ends up in a steady glide, if the engine power is cut and the stick is left free. Paper gliders on the other hand often go through a series of swooping dives broken by stalls, or spiral towards the ground in a spin.

During steady unpowered descent the air hits the aircraft from below at an angle γ with the horizontal, called the *glide angle*, corresponding to a *glide slope* $\tan \gamma$. The ratio of horizontal to vertical air speed is called the *glide ratio*, and equals the inverse of the glide slope, *i.e.* $\cot \gamma$. An aircraft can glide steadily with different airspeeds for a large range of angles of attack. The angle of attack that yields maximal glide ratio determines how far an aircraft at best can reach by gliding down from a given altitude, also called its *glide range*.

Typical commercial aircraft have best glide ratios of 10–20 with 17 for the Boeing 747 and 8 for the Concorde. So if the engines set out at an altitude of 10 km, the pilot has to look for a place to land inside 100 – 200 km, depending on the aircraft. These glide ratios are comparable to those of gliding birds like the swift (10) and soaring birds like the albatross (20). Modern sailplanes may reach glide ratios around 30–55 and in extreme cases even higher. The space shuttle, on the other hand, approaches the runway at a glide angle $\gamma = 19^\circ$, corresponding to a glide ratio of around 3. With its stubbed wings and large weight it is a rather bad glider, comparable to a sparrow. The human body is even worse, with a best glide ratio of about unity.

In steady unpowered descent the aerodynamic reaction force must be equal and opposite to the weight of the aircraft, or in size $\mathcal{R} = Mg_0$. Resolving the reaction force into lift and drag we find,

$$\mathcal{L} = Mg_0 \cos \gamma, \quad \mathcal{D} = Mg_0 \sin \gamma. \quad (27-10)$$

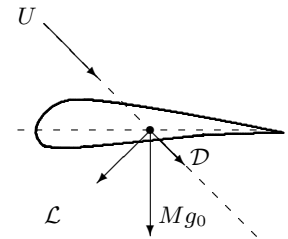
These equations could also have been obtained from the steady flight equations (27-8) with $T = 0$ and $\theta = -\gamma$. From the glide angle and the weight of an aircraft, we may thus determine both the lift and drag that acts on it in this flight condition. The glide ratio evidently equals the ratio of lift to drag in unpowered descent,

$$\cot \gamma = \frac{\mathcal{L}}{\mathcal{D}}. \quad (27-11)$$

Aerodynamics tells us (see the following section) that the ratio of lift to drag essentially only depends on the angle of attack, so the best glide ratio is obtained by choosing that angle of attack which maximizes \mathcal{L}/\mathcal{D} .

Notice that neither lift nor drag are horizontal in unpowered descent. The lift is tilted forward and the drag backwards.

The forward tilt of the lift also allows us to understand broadly how birds and insects generate thrust in level flight by flapping their wings straight up and down. In this unsteady flight mode, there is no instantaneous balance of aerodynamic forces and gravity, but during the downstroke, the air will hit the wing from below and generate a tilted lift, propelling the bird forward (and upwards), provided the drag is not too large. During upstroke the picture is inverted, and air hits the wing from above, but the lift is still tilted forwards and thus again propels the bird forwards, provided drag does not overwhelm it. Insects and birds that hover instead of flying horizontally get lift by interacting with vortices created at the leading edge of the wings during the downstroke and by other mechanisms².

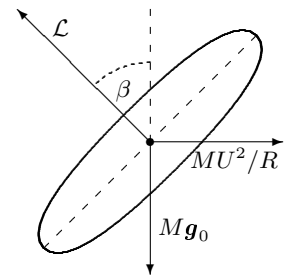


Sketch of forces during bird wing upstroke in forward flight. The total force does not vanish in this case, but accelerates the bird downwards. The lift provides forward thrust, when the drag is not too large.

Horizontal banked turn

Consider an aircraft flying steadily under power with velocity U in a horizontal circle of radius R . From the (rotating) rest frame of the aircraft, the air again flows steadily past with velocity U , but now there is also a centrifugal force MU^2/R directed away from the center of the circle. The engine thrust is assumed to balance the drag, and the lift must therefore balance the vector sum of the weight and the centrifugal force. Denoting by β the angle between the vertical and the lift vector, we obtain by projecting the lift on the horizontal as well as the vertical directions,

$$\mathcal{L} \cos \beta = Mg_0 \quad \mathcal{L} \sin \beta = \frac{MU^2}{R}. \quad (27-12)$$



Sketch of forces in the transverse plane during a steady horizontal banked turn, here with tilt angle $\beta \approx 45^\circ$.

²See for example R. B. Srygley and A. L. R. Thomas, *Unconventional lift-generating mechanisms in free-flying butterflies*, Nature **420**, 660 (2002) and references therein.

The lift divides out in the ratio of these equations, and we get

$$\tan \beta = \frac{U^2}{g_0 R}. \quad (27-13)$$

Airplanes are normally tilted (banked) through the precisely this angle β during turns, such that the floor of the aircraft remains orthogonal to the lift. In such a *clean turn*, the effective gravity experienced inside the airplane is (in units of the standard gravity)

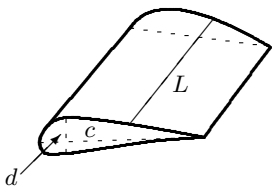
$$\frac{g_{\text{eff}}}{g_0} = \frac{\mathcal{L}}{Mg_0} = \frac{1}{\cos \beta}, \quad (27-14)$$

also called the *load factor* or the *g-factor*.

Example 27.3.2: In a clean 60° banked turn, one pulls a g -factor of 2. Fighter jets may generate g -factors up towards 10, corresponding to bank angles $\beta \lesssim 84^\circ$. To avoid passenger discomfort, most commercial aircraft rarely bank beyond 15° with a nearly imperceptible increase in load factor of about 3%. At a speed of 900 kilometers per hour and $\beta = 15^\circ$, the clean turn diameter is $2R = 2U^2 \cot \beta / g_0 \approx 50$ kilometers, and a full turn at this speed takes $T = 2\pi R / U \approx 10$ minutes.

27.4 Estimating lift

Aerodynamic lift in nearly ideal flow is almost entirely caused by pressure differences between the upper and lower wing surfaces. In this section we shall describe the basic physics of lift and estimate its properties from relatively simple physical arguments, and in the following section we shall make similar estimates of the various contributions to drag. It should however be borne in mind that we would rather want to calculate lift and drag from fluid mechanics, in terms of the angle of attack, velocity, air density, and the shape of the wing. Such theoretical knowledge makes it possible to predict which parameter intervals allow an aircraft to become airborne and sustain steady flight. In section 27.7 we explicitly calculate the lift for thin airfoils.



A wing is characterized by three lengths: the span L , the chord c , and the thickness d . The wing profile depicted here also carries aerodynamic twist.

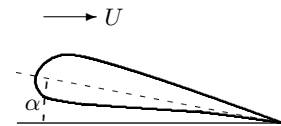
Wing and airfoil geometry

An airplane wing may be characterized by three different length scales: the tip-to-tip length or *span* L , the transverse width or *chord* c , and the thickness d . A wing can only in the coarsest of approximations be viewed as a rectangular box. Typically wings are both thin and long, $d \ll c \ll L$. Many wings *taper* towards the tip and are swept back towards the rear. Other wing shapes are also found, for example the delta-wing of the Concorde. For a rectangular wing, the dimensionless number L/c is called the *aspect ratio*. For tapering and unusually shaped wings, one may instead use the average cord length $c = A/L$, where A is the planiform area of the wing (the area of the wing's "shadow" on the

wing plane), so that the aspect ratio becomes $L/c = L^2/A$. The wing may furthermore twist slightly along the span leading to a varying angle of attack. This is in particular true for propellers that basically are wings mounted on a rotating shaft.

Example 27.4.1: The Boeing 747-400 has a wing span of $L \approx 64$ m and a wing area $A \approx 520$ m², leading to an average cord length of $c \approx 8$ m and an aspect ratio of $L/c \approx 8$. For comparison, the albatross with its narrow long wings has an aspect ratio of about 20, at par with modern sailplanes. At the extreme end one finds NASA's solar-cell powered flyer Helios which has an aspect ratio of nearly 31. Incidentally, a man with his arms stretched out as wings has an aspect ratio of about 20, so aspect ratio is not everything.

The transverse wing profile, also called the *airfoil*, is normally slightly curved, or *cambered*, along the cord, with a soft leading edge and a sharp trailing edge. The angle of attack of an airfoil is defined to be the angle between the asymptotic airflow and the *chord line* which is a straight line of length c connecting the leading and trailing edges. Depending on how the wings are attached to the aircraft there may be a small difference between the angles of attack of the wing and the aircraft.



The angle of attack for an airfoil is conventionally defined to be the angle between the airflow and chord line.

Average pressure difference

The chordwise Reynolds number,

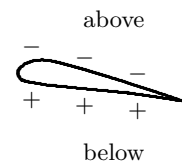
$$\text{Re}_c = \frac{Uc}{\nu}, \quad (27-15)$$

is an important dimensionless combination of the asymptotic flow speed U , the chord c , and the kinematic viscosity of air, $\nu = \eta/\rho_0$. The chordwise Reynolds number indicates the character of the airflow around the wing and will always be assumed to be very large, of the order of many millions, so that the flow pattern around the wings just outside the omnipresent boundary layers may be taken to be very nearly ideal with pressure completely dominating the stress tensor.

Consider now an airplane with almost planar wings flying horizontally under a small angle of attack. The only way pressure can lift the airplane is by being lower above the wing than below. The actual pressure varies around the wing (see fig. 27.1) but the average pressure difference between the upper and lower surfaces, also called the *wing loading*, may be estimated from the total aerodynamic lift on the wings and the total wing area A ,

$$\Delta p \approx -\frac{\mathcal{L}}{A}. \quad (27-16)$$

In steady level flight, lift equals weight, $\mathcal{L} = Mg_0$, as discussed in the preceding section, and wing loading is easy to calculate from aircraft dimensions and performance.



The pressure is lower above the wing than below. This is what carries the aircraft.

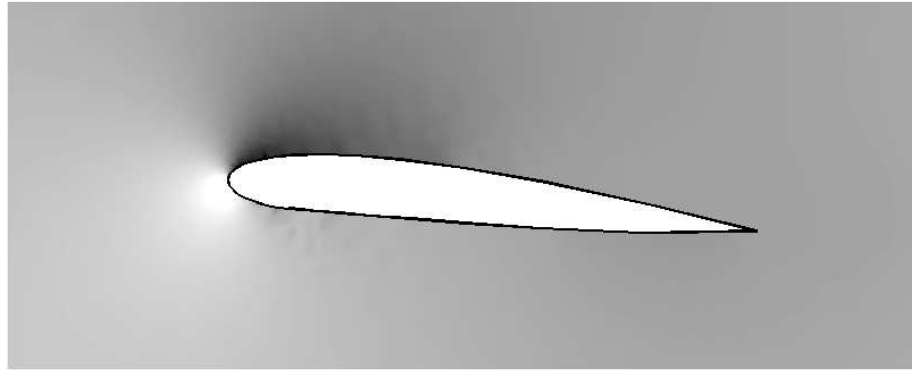


Figure 27.1: Pressure distribution around an airfoil at Reynolds number $Re_c = 10,000$ and angle of attack $\alpha \approx 6^\circ$, obtained by numeric simulation. Notice the higher stagnation pressure (light) at the leading edge and the lower lifting pressure (dark) above the wing. It typically acts about one quarter of the chord length downstream from the leading edge of the wing. The pressure below the wing is not much higher than the pressure at infinity.

Example 27.4.2: The cruising speed for the Boeing 747-400 is $U \approx 250$ m/s, and with an average chord length of $c \approx 8$ m, the chordwise Reynolds number becomes $Re_c \approx 2 \times 10^8$. The maximal takeoff mass is $M \approx 400,000$ kg distributed over a wing area of about $A \approx 520$ m², leading to a wing loading of about $\Delta p \approx 7,500$ Pa, which is only 7.5% of atmospheric pressure at sea level, but about 25% of the actual pressure at the normal cruising altitude of 10 km.

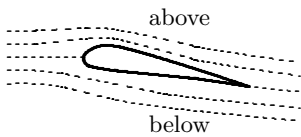
Average flow velocity difference

In nearly ideal flow, Bernoulli's theorem for incompressible fluids (16-16) may be used to relate the pressures and velocities above and below the wing. As discussed in section 16.4 on page 269, air is effectively incompressible at speeds much lower than the speed of sound, *i.e.* for small Mach number $Ma = v/v_{\text{sound}}$. This excludes us from discussing modern passenger jets flying at $Ma \approx 0.8$, but the following discussion is fine for $Ma \lesssim 0.3$.

Consider now two streamlines coming in from afar and passing on each side of the wing. Although they begin in different places, they start out with the same velocity U and pressure $p = P$, so that by Bernoulli's theorem,

$$\frac{P}{\rho_0} + \frac{1}{2}U^2 = \frac{p_{\text{above}}}{\rho_0} + \frac{1}{2}v_{\text{above}}^2 = \frac{p_{\text{below}}}{\rho_0} + \frac{1}{2}v_{\text{below}}^2. \quad (27-17)$$

From this we get the pressure difference between nearby points above and below



Sketch of streamlines around a wing with positive lift. The wing profile and angle of attack accelerates the flow across the top of the wing and retards it below, and thus creates a lower pressure above than below. Notice the presence of front and rear stagnation points with vanishing airspeed.

the wing,

$$\begin{aligned}\Delta p &= p_{\text{above}} - p_{\text{below}} = -\frac{1}{2}\rho_0(v_{\text{above}}^2 - v_{\text{below}}^2), \\ &\approx -\frac{1}{2}\rho_0(v_{\text{above}} + v_{\text{below}}) \cdot (v_{\text{above}} - v_{\text{below}}), \\ &\approx -\rho_0 U \Delta v,\end{aligned}$$

where $\Delta v = v_{\text{above}} - v_{\text{below}}$ is the local velocity difference. In the last line we have assumed that the local velocity difference is much smaller than the mainstream velocity, $\Delta v \ll U$, and that the flow velocity over most of the wing surface cannot deviate much from the mainstream velocity, *i.e.* $v_{\text{above}} \approx v_{\text{below}} \approx U$. This assumption must necessarily break down near the leading and trailing ends of the wing, where there are stagnation points with vanishing flow speed. For a sufficiently thin planar wing, these end effects can be disregarded in our estimate.

Combining this result with (27-16) we obtain an estimate of the (average) flow velocity difference in units of the mainstream velocity

$$\frac{\Delta v}{U} \approx -\frac{\Delta p}{\rho_0 U^2} \approx \frac{\mathcal{L}}{\rho_0 U^2 A}. \quad (27-18)$$

Again this is easy to estimate from aircraft dimensions and performance data, using that $\mathcal{L} = M g_0$ for level flight.

Example 27.4.3 (Cessna 150): The popular Cessna 150 two-seater has a wing span of $L \approx 10$ m, wing area $A \approx 15$ m², and thus an average chord of $c \approx 1.5$ m, and an aspect ratio of $L/c \approx 6.7$. With a maximum takeoff mass of $M \approx 700$ kg, the wing loading becomes $\Delta p \approx 460$ Pa which is merely 0.5% of atmospheric pressure at sea level. At cruising speed $U \approx 200$ km/h = 55 m/s, the Reynolds number is $\text{Re}_c \approx 5 \times 10^6$. The Mach number is $\text{Ma} \approx 0.17$, and the average velocity difference between the upper and lower wing surfaces $\Delta v \approx 8.5$ m/s, or $\Delta v/U \approx 0.15$.

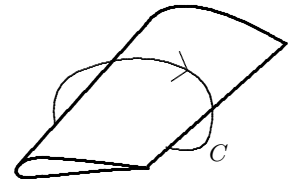
Circulation and lift

The difference in flow velocity between the wing surfaces (outside the boundary layers) not only gives rise to a pressure difference and thereby lift, but also generates a circulation which can be estimated from the (average) velocity difference

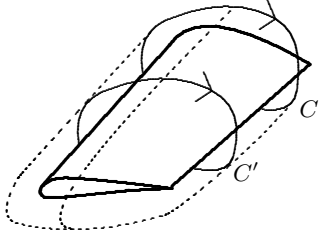
$$\Gamma = \oint_C \mathbf{v} \cdot d\boldsymbol{\ell} \approx c v_{\text{above}} - c v_{\text{below}} = c \Delta v.$$

Here the sign is determined by letting the contour C circle the wing in the direction of the asymptotic airflow \mathbf{U} on top and against it below (just outside the boundary layers). Using (27-18) we obtain the relation,

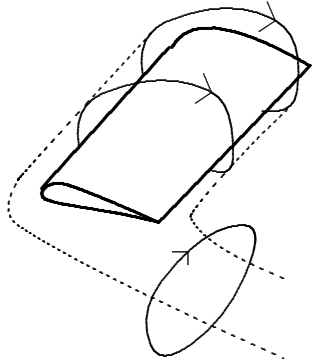
$$\boxed{\mathcal{L} \approx \rho_0 U L \Gamma}. \quad (27-19)$$



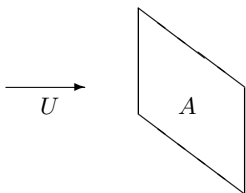
The integration contour for circulation.



Sketch of vortex bound to the (left) wing of an aircraft. The circulation is the same for the two curves C and C' , provided there is no flux of vorticity through the surface bounded by these curves. Notice how C' can be slid off the tip of the wing and shrunk to a point if the flow is truly irrotational (which it therefore cannot be).



The bound vortex turning into a trailing vortex at the wing tip.



The momentum flux through the area A from the uniform flow with velocity U is the product of the momentum density $\rho_0 U$ and the volume flux UA .

This is the famous *Kutta-Joukowski* theorem from the beginning of the twentieth century relating lift and circulation. Although derived here from coarse estimates, we shall see in section 27.6 that in nearly ideal irrotational flow around an infinitely long wing with constant chord length this relation is in fact exact. The realization that lift and circulation are two sides of the same coin, was probably *the single most important insight into the mechanics of flight*. With this in hand, the road was opened for calculating the lift produced by any specific airfoil for which the circulation could be obtained, analytically or numerically.

The horseshoe vortex system

In nearly ideal irrotational flow, the circulation is the same around any curve encircling the wing, because Stokes' theorem relates the difference in circulation between two such curves to the flux of vorticity (which is assumed to vanish) through the surface bounded by the two curves. The lift-generating circulation thus forms a *bound vortex* that ideally cannot leave the wing. For an infinitely long wing this creates no problem, but for a wing of finite span, the assumption of vanishing vorticity has to break down, because one of the curves may be "slid over" the tip of the wing and shrunk to a point with no circulation. The inescapable conclusion is that since lift requires non-zero circulation, vorticity must come off somewhere along the finite span of a real wing.

The shedding of vorticity from a wing of finite span depends strongly on its shape. A wing that tapers towards the tip will shed vorticity everywhere along its trailing edge, though most near the tip. If the wing is rectangular with constant chord, the vorticity will tend to appear very close to the tip. In any case, the vorticity coming off the tip is turned backwards with respect to the direction of flight, forming a *trailing vortex* in continuation of the bound vortex. Alternatively one may see the trailing vortex as created by the flow around the tip from below to above the wing, seeking to equalize the higher pressure underneath the wing with the lower pressure above. Together with the bound vortex the two trailing vortices coming off the wing tips form a horseshoe-shaped vortex system associated with all winged aircraft in flight.

Lift coefficient

The dimensionless quantity on the right hand side of (27-18) is of great importance for flight. Conventionally, the *lift coefficient* of a wing is defined to be twice as large, and written

$$C_L = \frac{\mathcal{L}}{\frac{1}{2}\rho_0 U^2 A}. \quad (27-20)$$

The denominator is proportional to the momentum flux $\rho_0 U \cdot UA$ through an area A orthogonal to the mainstream direction, and thus sets the scale for the total force that the incoming airstream can exert on this area. The factor $1/2$

in the denominator is conventional (although some justification is given in the following section).

Being dimensionless, the lift coefficient can only depend on dimensionless quantities, such as the angle of attack α , the Reynolds number $\text{Re}_c = Uc/\nu$, the aspect ratio L/c , and other quantities characterizing the shape of the wing. The mainly empirical studies by scientists and engineers in the 19'th century, up to and including the Wright brothers, led to the understanding that the angle of attack was the decisive parameter in the lift coefficient. The dependence on the other dimensionless parameters was found to be weaker, in fact so weak that it was mostly ignored before 1900.

The weak dependence of the lift coefficient on the Reynolds number allows us to conclude that the lift itself,

$$\mathcal{L} \approx \frac{1}{2} \rho_0 U^2 A C_L, \quad (27-21)$$

is directly proportional to the square of the velocity. At takeoff and especially during approach to landing, where speeds are low, the pilot can increase the wing area by means of *flaps*. Since lift always nearly equals weight, it follows from this expression that the increase in area will be compensated by a decrease in required airspeed (for a fixed angle of attack). Fully extended flaps also have a considerably larger angle of attack than the wing itself, increasing thereby the lift coefficient and leading to a further reduction in the required landing speed.

Dependence on angle of attack

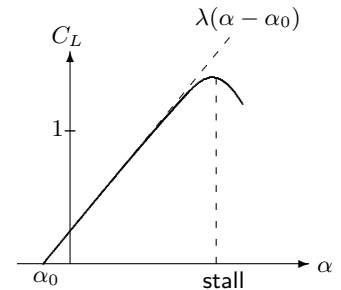
Empirically, the lift coefficient is surprisingly linear in the angle of attack,

$$C_L \approx \lambda (\alpha - \alpha_0), \quad (27-22)$$

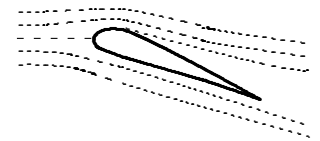
where $\lambda = dC_L/d\alpha$ is called the *lift slope*, and α_0 is the angle of attack at which the lift vanishes. In section 27.7 we shall see theoretically that for thin airfoils the slope is universally $\lambda = 2\pi$ (with the angle of attack measured in radians). The zero-lift angle α_0 depends mainly on the shape of the airfoil, and is usually small and negative, for example $\alpha_0 \approx -2^\circ$ (see example 27.4.3).

It follows from the above equations and the constancy of required lift that the relative angle of attack $\alpha - \alpha_0$ must vary inversely with the square of the velocity, $\alpha - \alpha_0 \sim 1/U^2$. The rapid rise of the required angle of attack with decreasing airspeed leads quickly to boundary layer separation on the wing, accompanied by a dramatic loss of lift and increase in drag. This phenomenon is called *stall*, and happens typically at a critical angle of attack, the stall angle $\alpha_{\text{stall}} \approx 15 - 20^\circ$ for normal aircraft. Whereas the lift slope and zero-lift angle are essentially independent of the Reynolds number in the linear regime, the stall angle increases a bit with the increasing Reynolds number.

For special aircraft the stall angle can be fairly high, for example 35° for delta-winged aircraft such as the space-shuttle or the Concorde. The higher stall angle



Sketch of a lift curve rising linearly until it veers off rather sharply at an angle of typically $15 - 20^\circ$, signalling stall. Beyond this angle, lift drops precipitously, and so does the airplane.



Sketch of the flow around an airfoil at large angle of attack. The boundary layer separates near the leading edge and replaces the previously laminar flow above the wing with turbulent flow yielding small lift and large drag.

is offset by a smaller lift slope, say $\lambda \approx 3$ (per radian) rather than 2π . In order to get sufficient lift, such aircraft are forced to take off and land under remarkably high angles of attack.

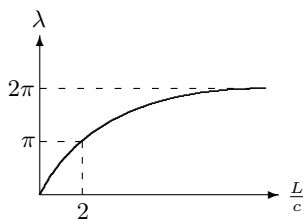
Dependence on aspect ratio

The shedding of vorticity from finite wings makes the lift slope depend on the aspect ratio L/c . An expression useful for estimating this effect for thin airfoils is [53, p. 380]

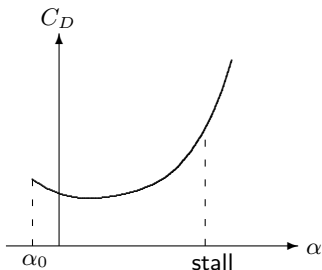
$$\lambda \approx \frac{2\pi}{1 + 2\frac{c}{L}}, \quad (27-23)$$

which in the limit of infinite aspect ratio, $L/c \rightarrow \infty$, converges upon 2π .

Example 27.4.4 (Cessna 150): For the Cessna 150 (page 549) at cruising speed $U = 200$ km/h we estimated $\Delta v/U \approx 0.15$, implying a lift coefficient $C_L \approx 0.3$. With aspect ratio $L/c \approx 8$ the lift slope is $\lambda \approx 5$, and the relative angle of attack becomes $\alpha - \alpha_0 \approx 0.06 \approx 3.5^\circ$, and since $\alpha_0 \approx -2^\circ$ for this airfoil, the true angle of attack becomes $\alpha \approx 1.5^\circ$. At half the cruising velocity, *i.e.* for $U = 100$ km/h, the relative angle of attack is four times larger, *i.e.* 14° , and the true angle of attack 12° . Since the stall angle is 16° for this airfoil, stall is imminent when the speed drops below about 85 km/h.



Sketch of the variation of the lift slope with aspect ratio.



Sketch of a typical drag curve for a cambered airfoil as a function of angle of attack. Notice that the drag of such an airfoil actually decreases for small angles of attack. Beyond the critical angle of attack, the drag coefficient rises steeply.

27.5 Estimating drag

Whereas lift has but one cause, *i.e.* the pressure difference between the upper and lower wing surfaces, drag has several. First, there is skin friction from the air flowing over the wing. Second, there is form drag due to the wing obstructing the free air flow and leaving a trail of turbulent air behind, and third there is induced drag coming from the vortices that always trail the wing tips. For real aircraft, the body shape and various protrusions (radio antenna, Pitot tube) also add to drag. As for lift, it is convenient and customary to discuss drag in terms of the dimensionless drag coefficient

$$C_D = \frac{\mathcal{D}}{\frac{1}{2}\rho_0 U^2 A}, \quad (27-24)$$

which has the same denominator as the lift coefficient (27-20).

The denominator can be understood in the following way. At the leading edge of a wing there is always a streamline that ends with vanishing airspeed (stagnation). The pressure increase at the stagnation point relative to infinity is $\Delta p_{\text{stag}} = \frac{1}{2}\rho_0 U^2$, according to Bernoulli's theorem. If the wing were raised squarely into the oncoming airflow, it would present an area A to this pressure, and assuming that the turbulent "dead" air behind the wing exerts essentially no extra pressure

on the back of the wing, the total drag force would be $\Delta p_{\text{stag}} A = \frac{1}{2} \rho_0 U^2 A$, which is the denominator. If this argument is right, we predict $C_D \approx 1$ for a thin flat plate with its face into the wind, and that agrees in fact quite reasonably with both theory and experiment. For a circular disc we thus have $C_D = 1.17$ (see section 20.4 on page 388). That the true drag coefficient is larger than unity can be interpreted as the average true pressure drop across the disc being smaller than Δp_{stag} .



The stagnating streamline at the leading edge terminates with zero flow velocity. Bernoulli's theorem implies that the pressure increase at the forward stagnation point is $\Delta p_{\text{stag}} = \frac{1}{2} \rho_0 U^2$.

Skin friction

Close to the wing surfaces there are thin boundary layers (see chapter 25 on page 483), in which the flow velocity changes rapidly from zero right at the skin of the wing to the mainstream airspeed just outside. The maximal thickness of the boundary layer on a wing may be estimated from the flat plate laminar Blasius solution (25-28) or from semi-empirical turbulent expression (25-41),

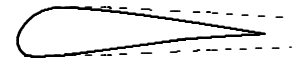
$$\frac{\delta}{c} \approx \begin{cases} 5 \text{Re}_c^{-1/2} & \text{laminar} \\ 0.16 \text{Re}_c^{-1/7} & \text{turbulent} \end{cases} \quad (27-25)$$

Boundary layers do not have the same thickness everywhere on the wing surface, but are generally thinnest at the leading edge of the wing and become thicker towards the rear. Usually, the Reynolds number is so high that the boundary layers also develop turbulence somewhere downstream from the leading edge. For aircraft with chordwise Reynolds numbers in the millions and chords of the order of meters, a fully laminar boundary layer is only millimeters thick whereas a fully turbulent layer is an order of magnitude thicker.

To estimate the skin friction we again use flat-plate Blasius' result (25-32) in the laminar regime and the semi-empirical expression (25-34) in the turbulent,

$$C_D^{\text{skin}} = \frac{D_{\text{skin}}}{\frac{1}{2} \rho_0 U^2 A} \approx \begin{cases} 2.65 \text{Re}_c^{-1/2} & \text{laminar} \\ 0.063 \text{Re}_c^{-1/7} & \text{turbulent} \end{cases} \quad (27-26)$$

Notice that this is roughly half the relative thickness estimate (27-25). The skin drag coefficient always decreases with increasing Reynolds number, but like the thickness it varies much slower in the turbulent region than in the laminar. Turbulent drag is considerably larger than laminar drag, but precise theoretical prediction of skin drag is quite hard because it is difficult to predict the line along the span where the boundary layer becomes turbulent. This is one of the reasons that wind tunnel experiments, and in more recent times numeric (CFD) simulations, have been and still are so important for aerodynamics engineering.



Boundary layers thicken and become turbulent towards the rear of the wing and leave a trailing turbulent wake behind. The thickness of the trailing wake is comparable to the boundary layer thickness (here strongly exaggerated).

Example 27.5.1: For the Cessna 150 of example 27.4.3 at cruising speed with $\text{Re}_c \approx 5 \times 10^6$, the estimate of the maximal laminar boundary layer thickness becomes $\delta \approx 3.5 \text{ mm}$ whereas the estimate of the maximal turbulent thickness becomes $\delta \approx 27 \text{ mm}$. The corresponding laminar skin drag coefficient is $C_D^{\text{skin}} \approx 0.0012$ whereas the turbulent one is about six times larger, $C_D^{\text{skin}} \approx 0.0070$. In view of the large Reynolds number, the truth presumably lies close to the larger value.

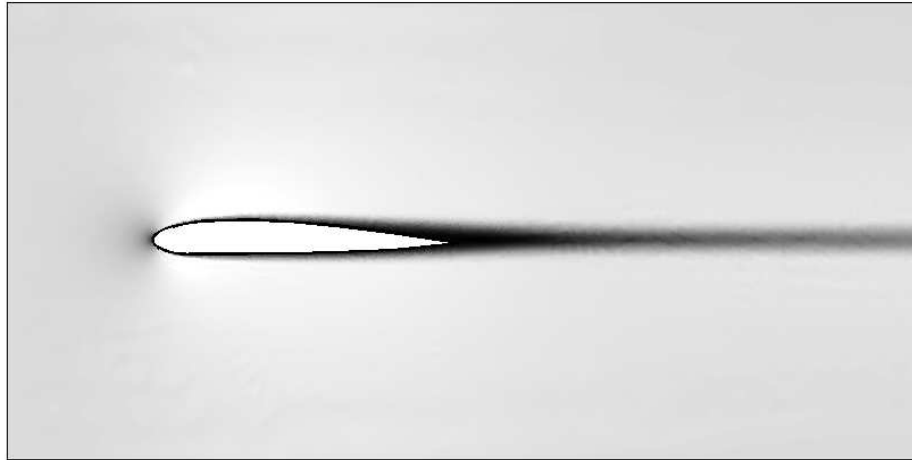


Figure 27.2: *Horizontal velocity distribution (v_x) around an airfoil at Reynolds number $Re_c = 10,000$ and $\alpha \approx 1^\circ$, obtained by numeric simulation. Notice the faster flow above the wing (light), the stagnating flow at the leading edge (dark), and the strong slowdown of the flow in the boundary layers and the trailing wake (very dark). The boundary layers are thin and laminar, thicken towards the rear especially on the upper surface where the initial acceleration of the air is followed by deceleration. There is no turbulence in the boundary layers at a Reynolds number as low as here. At more realistic Reynolds numbers in the millions, the boundary layers are mostly turbulent and about an order of magnitude thinner than here. Well behind the airfoil the wake has a thickness comparable to the boundary layers. The slow viscous expansion of the laminar wake is not visible at the scale of this figure.*

Form drag

The flow around a highly streamlined body, such as a thin wing narrowing down into a sharp trailing edge, will be nearly ideal everywhere, except in the boundary layers. It has been pointed out before (and we shall prove it in the following section) that a body in a truly ideal, irrotational flow does not experience any drag at all, independently of its shape. Both skin friction and form drag therefore owe their existence to viscosity, but where skin friction is due to shear stresses in the boundary layer, form drag arises from changes in the pressure distribution over the body caused by the presence of boundary layers.

Airfoil boundary layers tend to become turbulent at some point downstream from the leading edge of the wing. At the sharp trailing edge the boundary layers separate from the wing and continue as a *trailing wake* of essentially infinite extent after the wing (see figs. 27.2 and 27.3). The unsteady turbulent wake found immediately behind the trailing edge of a wing expands slowly and eventually calms down and becomes steady and laminar at some downstream distance from the wing. Further downstream the laminar wake continues to expand by viscous diffusion at a considerably faster rate than the turbulent wake. In section 27.8 we shall determine the general form of the field in the distant laminar wake.

Inside the trailing wake immediately behind the body the pressure will be lower than the stagnation pressure $\Delta p_{\text{stag}} = \frac{1}{2}\rho_0 U^2$ at the leading edge (see fig. 27.1) and this pressure difference is the cause of drag. The thickness of the turbulent wake immediately after the trailing edge of the wing may be estimated from the boundary layer thickness δ , leading to the form drag estimate $D_{\text{form}} \sim \Delta p_{\text{stag}} L \delta$. In terms of the drag coefficient we thus find for the turbulent case,

$$C_D^{\text{form}} \sim \frac{\delta}{c} \sim \text{Re}_c^{-1/7} \quad (27-27)$$

Form drag usually amounts to some fraction of skin friction for streamlined objects where the boundary layers are thin everywhere.

With growing angle of attack, flow separation may occur on the upper side of the wing at some point before the trailing edge of the airfoil, thereby increasing form drag and diminishing lift. At a certain angle of attack, the point of separation for the turbulent boundary layer on the top side of the wing may suddenly shift forward from the trailing edge, creating a highly turbulent region everywhere above the wing. This leads to loss of almost all of the lift and at the same time an increased drag. The wing and the aircraft are then said to have *stalled*.

The efforts of aircraft designers between the world wars in the 20'th century were mainly directed towards form drag reduction by streamlining. A smaller drag generally implies higher top speed, greater payload capacity, and better fuel economy. Besides streamlining of lift surfaces, drag reduction was also accomplished by internalizing the wing support structure and the undercarriage, and providing the engines with carefully designed cowlings.

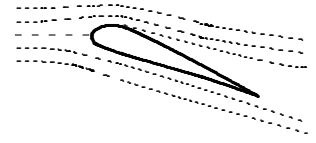
Induced drag

The two vortices trailing from the wing tips of an aircraft rotate in opposite directions and carry roughly the same circulation Γ as the vortex bound to the wing. They are created at a rate determined by the speed U of the airplane and persist indefinitely in a truly ideal fluid. In a viscous fluid they spin down and dissolve after a certain time.

The process of “spinning up” and “feeding out” the trailing vortices from the wing-tips of the aircraft is accompanied by a continuous loss of energy, which causes an extra drag on the aircraft. We can estimate the order of magnitude of this drag from the kinetic energy contained in a vortex with circulation Γ and core radius a . Since the maximal flow speed is of order $v_\phi \sim \Gamma/2\pi a$, the kinetic energy of two vortex segments of length b becomes of magnitude $\mathcal{T} \sim \rho_0 v_\phi^2 \pi a^2 b \sim \rho_0 \Gamma^2 b$ (dropping all simple numeric factors). This loss of energy must cause a drag on the aircraft of magnitude

$$D_{\text{induced}} = \frac{\mathcal{T}}{b} \sim \rho_0 \Gamma^2 \sim \rho_0 U^2 c^2 C_L^2,$$

where we in the last estimate have used the relation between lift and circulation (27-19) and the definition of the lift coefficient (27-20). The estimate of the



Sketch of the flow around an airfoil at large angle of attack. The boundary layer separates near the leading edge and replaces the previously laminar flow above the wing with turbulent flow yielding small lift and large drag.

induced drag coefficient thus becomes

$$C_D^{\text{induced}} = \frac{D_{\text{induced}}}{\frac{1}{2}\rho_0 U^2 A} \sim \frac{c}{L} C_L^2. \quad (27-28)$$

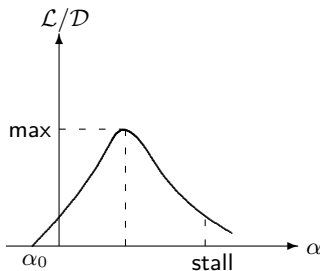
Classical wing theory yields an expression of precisely this form but roughly a factor π smaller. Since induced drag is a byproduct of the lift-generating flow around a finite wing, it is also called *drag due to lift*. It is the unavoidable price to pay for wings of finite span.

Induced drag is normally smaller than skin drag, but grows rapidly with increased angle of attack and may win over skin drag at low speeds at, for example, takeoff and landing where the angle of attack is large and the skin friction small. Most importantly, induced drag decreases with increasing aspect ratio L/c , explaining why large aspect ratios are preferable, up to the point where the sheer length of the wing begins to compromise the strength of the wing structure.

Example 27.5.2: For the Cessna 150 of example 27.5.1 cruising in level flight with $C_L \approx 0.3$ and aspect ratio 8 we find $C_{\text{induced}} = 0.0036$ (including the factor $1/\pi$). The induced drag is thus about half of turbulent skin drag. At half this speed the angle of attack is four times bigger, so that the induced drag coefficient becomes 16 times bigger whereas the turbulent skin drag coefficient stays roughly constant.

Lift-to-drag ratio

The total drag coefficient C_D is the sum of all the contributions from various sources: skin drag, form drag, induced drag, etc. The lift-to-drag ratio, $\mathcal{L}/\mathcal{D} = C_L/C_D$, is a measure of the *aerodynamic efficiency* of an airplane. Like lift and drag, it is strongly dependent on the angle of attack and less on the Reynolds number and aspect ratio. The quadratic growth of induced drag as a function of angle of attack normally overcomes the linear rise in lift and creates a maximum in \mathcal{L}/\mathcal{D} for a certain angle of attack, typically at about half the stall angle. We have seen earlier, that in a steady glide the best glide ratio (27-11) is obtained for an angle of attack given by the maximal value of lift-to-drag. In view of the problems in calculating drag with some confidence, empirical lift-to-drag curves are usually plotted for particular airplanes to document their performance.



Sketch of a typical lift-to-drag curve for an airplane. The maximal value of lift to drag determines the best glide ratio.

Example 27.5.3: For the Cessna 150 of the preceding examples cruising in level flight with $C_L \approx 0.3$ and aspect ratio 8 we estimate the different contributions to drag as 0.007 from skin friction, 0.007 from form drag, and 0.004 from induced drag. The total drag coefficient becomes thus 0.018, corresponding to a lift-to-drag ratio of $\mathcal{L}/\mathcal{D} = 17$. This is an overestimate by about a factor of two compared to the actual performance of this aircraft which has a quoted glide ratio of about 8. The reason is that in our calculation of drag we have left out the contributions from the passenger compartment, the fixed undercarriage with wheels, the struts supporting the wing, and other features that increase drag.

* 27.6 Lift, drag, and the trailing wake

An often recurring question that can lead to heated discussions is whether an airplane stays aloft in steady flight because of the pressure differences between the upper and lower wing surfaces, or whether it gets lift from diverting momentum downwards. The general treatment of momentum balance in section 17.5 on page 296 indicates that the total contact force on the airplane should be balanced by an opposite momentum flux at great distances, where all stresses have died away. Either position is in fact tenable in a discussion, but as we shall see the correct answer is more subtle than might be guessed at first glance.

Momentum balance in a box

Let the steadily moving body — an aircraft or wing — be surrounded with a huge imaginary “box” S (of any shape), and let the volume of air between the body surface and the box be our control volume. As can be seen from fig. 27.3 this box will cut through the trailing wake somewhere behind the body. Disregarding gravity, the only forces acting on the control volume of air are the contact forces on the two bounding surfaces: the body and the box. At the body surface, the force on the air is the opposite of the reaction force \mathcal{R} on the body given by the integral (27-2), and at the box surface the “air-to-air” reaction force \mathcal{R}_S is an analogous integral over the stresses acting on the surface of the box.

In steady flow the total momentum of the air contained in the control volume remains constant, apart from tiny time-dependent contributions from the fluctuating velocity field in the turbulent wake, which we shall ignore here. Since there can be no momentum flux through the impermeable surface of the body, it follows from momentum balance (17-14) that the total force on the air in the control volume must equal the flux of momentum out of the box, or

$$\mathcal{R}_S - \mathcal{R} = \oint_S \rho_0 \mathbf{v} \cdot d\mathbf{S}$$

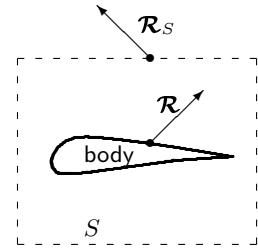
Expressing the box reaction force by an integral over the stress tensor, we find

$$\mathcal{R} = -\rho_0 \oint_S \mathbf{v} \cdot d\mathbf{S} + \oint_S \boldsymbol{\sigma} \cdot d\mathbf{S}, \quad (27-29)$$

where $\boldsymbol{\sigma} = \{\sigma_{ij}\}$ is the matrix form of the stress tensor $\sigma_{ij} = -p\delta_{ij} + \eta(\nabla_i v_j + \nabla_j v_i)$. The reaction force on the body can thus be calculated from the pressure and velocity fields, all evaluated at the surface of the box. It must be emphasized that this result is exact, valid for any shape and size of the body and box.

Box at spatial infinity

Let now the box expand to huge distances in all directions such that the velocity field on its surface approaches the asymptotic value, $\mathbf{v} \rightarrow \mathbf{U}$. Putting $\mathbf{v} = \mathbf{U} + \Delta\mathbf{v}$



Streamlined body and enclosing box S . The box needs not be rectangular like here but can be a volume of any shape. The reaction forces on body and box are for illustration purposes set to act in arbitrarily chosen points on the surfaces.

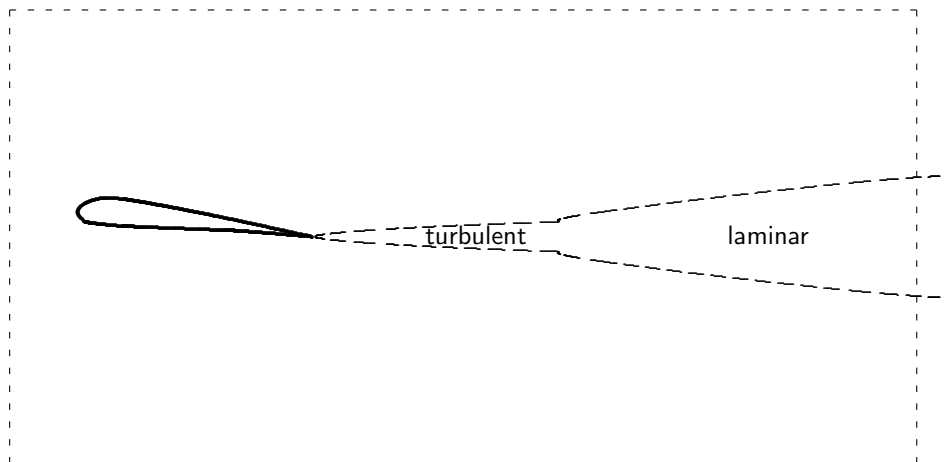


Figure 27.3: Sketch of a body (airfoil) and its trailing wake. Initially the trailing wake is turbulent, but expands slowly and becomes laminar some distance downstream. The thickness of the wake is greatly exaggerated compared to the distance from the body. The dashed box surrounding the system (but crossing through the trailing wake) is used in the text to define a control volume of air between the surfaces of the body and the box.

in the first (momentum) term of (27-29), it becomes

$$-\rho_0 \oint_S (\mathbf{U}\mathbf{U} + \mathbf{U}\Delta\mathbf{v} + \Delta\mathbf{v}\mathbf{U} + \Delta\mathbf{v}\Delta\mathbf{v}) \cdot d\mathbf{S}$$

Using that the total vector area of a closed surface always vanishes, $\oint d\mathbf{S} = \mathbf{0}$, together with global mass conservation, $\oint \Delta\mathbf{v} \cdot d\mathbf{S} = 0$, the first two terms in the integrand do not contribute to the integral. The last term is quadratic in the small velocity differences $\Delta\mathbf{v}$, so the conclusion is that only the third (linear) term in the momentum integral can survive in the limit of an infinite box.

If we think of the “box” as a huge sphere with radius r and surface area $4\pi r^2$, the velocity field must behave like $|\Delta\mathbf{v}| \sim 1/r^2$ at infinity³. The velocity derivatives in the stress tensor must then vanish like $|\nabla\Delta\mathbf{v}| \sim 1/r^3$, and cannot contribute to the second (force) term in (27-29). Pressure is thus the only stress component that has a possibility for surviving in the limit of an infinite box, so that the reaction force on the body may be written,

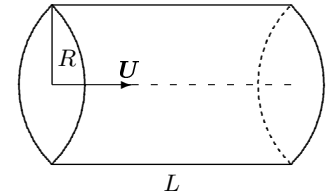
$$\mathcal{R} = -\rho_0 \oint_S \Delta\mathbf{v}\mathbf{U} \cdot d\mathbf{S} - \oint_S p d\mathbf{S} . \quad (27-30)$$

A constant pressure gives no contribution, and we may without loss of generality assume that the pressure vanishes at infinity at least as fast as $|p| \sim 1/r^2$.

³Outside the trailing wake! Inside the wake the velocity field behaves differently (see section 27.8) but the general conclusions remain valid.

We are now in position to answer the question of whether there remains a pressure contribution to lift far from the moving body. Although the derivation of the above equation shows that the *sum* of the pressure and momentum flow contributions is independent of the choice of the box shape, each term by itself will depend on it. Thus, *the limiting value of the pressure contribution may depend on how the box is taken to infinity.*

If we for example choose a cube or sphere and let it expand uniformly in all directions, there will usually be a residual pressure contribution to lift, even in the limit of an infinite box (see section 27.8 for an explicit calculation). Alternatively, one may choose a box in the form of a huge cylinder with radius R and length L , oriented with its axis parallel to the asymptotic flow \mathbf{U} . The pressure integral over the end caps cannot contribute to lift, because they are orthogonal to the velocity. If we now let the radius R become infinite, *before* the end caps are moved off to infinity, the pressure integral over the cylinder surface will behave like the area $2\pi LR$ times the pressure $p \sim 1/R^2$. It thus vanishes like L/R for $R \rightarrow \infty$ followed by $L \rightarrow \infty$, leaving no pressure contribution to lift in the limit.



Box in the shape of a cylinder of radius R and length L with axis parallel to the asymptotic velocity \mathbf{U} .

Lift and drag

Let us rearrange (27-30) in the form

$$\mathbf{R} = -\rho_0 \oint_S \mathbf{U} \times (\Delta \mathbf{v} \times d\mathbf{S}) - \oint_S (p + \rho_0 \Delta \mathbf{v} \cdot \mathbf{U}) d\mathbf{S} . \quad (27-31)$$

The first integral is evidently orthogonal to the asymptotic velocity and represents a pure lift,

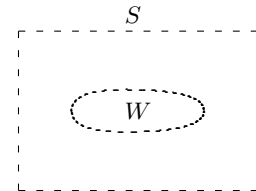
$$\mathcal{L} = -\rho_0 \oint_S \mathbf{U} \times (\mathbf{v} \times d\mathbf{S}) . \quad (27-32)$$

Here we have also replaced $\Delta \mathbf{v}$ by \mathbf{v} , using that $\oint d\mathbf{S} = \mathbf{0}$.

In regions where the flow is irrotational and streamlines connect to spatial infinity, the pressure is determined by Bernoulli's theorem, $p = \frac{1}{2}\rho_0(\mathbf{U}^2 - \mathbf{v}^2) \approx -\rho_0 \mathbf{U} \cdot \Delta \mathbf{v}$. Thus the integrand of the second term in \mathbf{R} vanishes in all regions where the flow is irrotational, *i.e.* outside the wake and the boundary layers. The contributions to the second integral can only come from the region W , where the box cuts through the wake. Choosing W to be planar and orthogonal to \mathbf{U} , its surface element $d\mathbf{S}$ will be parallel with \mathbf{U} , and the second term becomes a pure drag,

$$\mathcal{D} = - \int_W (p + \rho_0 \Delta \mathbf{v} \cdot \mathbf{U}) dS , \quad (27-33)$$

where dS is the area element of W . If we lift the restriction that W is a planar part of S orthogonal to \mathbf{U} , these formulas for lift and drag become slightly different (problem 27.4). Otherwise they are valid for all kinds of bodies moving steadily through a fluid at subsonic speed.



The downstream face of the box cuts the wake in a region W chosen to be orthogonal to the asymptotic flow \mathbf{U} .

d'Alembert's paradox: a gift to powered flight

We have previously (page 283) shown that a cylinder or sphere in irrotational (potential) flow experiences no drag. In irrotational flow, Bernoulli's theorem is fulfilled everywhere, so that the drag (27-33) must vanish. D'Alembert's paradox must be valid in full generality: *there is no drag on a body of arbitrary shape in completely irrotational flow*. But bodies moving through viscous fluid cannot help leaving a narrow trailing wake containing vorticity, and eq. (27-33) immediately resolves the paradox: *the drag on a body stems entirely from the trailing wake*.

In general the drag will be smaller, the narrower the wake. As we have seen in the estimates of the preceding section, drag is typically an order of magnitude smaller than lift for properly streamlined bodies, such as airfoils. This indicates that one should rather treat d'Alembert's "paradox" as a *theorem* about the near vanishing of drag for streamlined bodies at high Reynolds number. This theorem is in fact what makes flying technically possible with engines producing a thrust much smaller than the weight of the aircraft. Without d'Alembert's theorem, the Wright brothers would never have had a chance of flying at Kitty Hawk in December 1903, given the puny engine power then available to them.

Lift and vorticity

The box S used in the lift integral (27-32) is assumed to be of essentially infinite size. Let now S' be another closed surface surrounding the body somewhere inside the box S . From Gauss' theorem we obtain

$$\left(\oint_S - \oint_{S'} \right) \mathbf{U} \times (\mathbf{v} \times d\mathbf{S}) = - \int_V \mathbf{U} \times (\nabla \times \mathbf{v}) dV = - \int_V \mathbf{U} \times \boldsymbol{\omega} dV ,$$

where V is the region between the two surfaces, and $\boldsymbol{\omega} = \nabla \times \mathbf{v}$ is the vorticity field. In the extreme case we may take S' to be the body surface itself, where the velocity and thus the integral over S' vanishes because of the no-slip condition. It then follows from the above equation that the lift (27-32) is also given by the integral of the vorticity field over all of space,

$$\boxed{\mathcal{L} = \rho_0 \mathbf{U} \times \int \boldsymbol{\omega} dV} . \quad (27-34)$$

This integral can only receive contributions from the regions of non-vanishing vorticity, *i.e.* from the boundary layers and the trailing wake. Without vorticity created by friction, there can be no lift!

More generally, if there is no vorticity found in V , the integral over the box S equals the integral over S' . The original box may in other words be deformed into any other closed surface as long as it crosses no region containing vorticity. The box at infinity has now served its purpose and may be forgotten. In the following the surface S in (27-32) may be taken to be simply any surface surrounding the body, as long as there is no vorticity *outside* S .

Lift and circulation

It is useful to introduce a “natural” coordinate system with the x -axis along the direction of the asymptotic velocity $\mathbf{U} = U\mathbf{e}_x$ and the y -axis along the lift $\mathcal{L} = \mathcal{L}\mathbf{e}_y$. Working out the cross products, the lift (27-32) becomes

$$\mathcal{L} = \rho_0 U \oint_S (\mathbf{v} \times d\mathbf{S})_z = \rho_0 U \oint_S v_x dS_y - v_y dS_x, \tag{27-35}$$

together with the condition

$$\oint_S v_x dS_z - v_z dS_x = 0, \tag{27-36}$$

expressing that there should be no lift along the z -direction. For a symmetric aircraft in normal horizontal flight, this condition is automatically fulfilled.

The closed surface S may always be sliced into a set of planar closed contours $C(z)$ parallel with the xy -plane, and parameterized by the z -coordinate in some interval $z_1 \leq z \leq z_2$. The contours are given negative orientation in the xy -plane, *i.e.* clockwise as seen from positive z -values. Let now $d\boldsymbol{\ell} = (dx, dy, 0)$ be a line element on a point of the curve $C(z)$; it is evidently a tangent vector to the surface S . Let $d\mathbf{s} = (0, dy, dz)$ be another tangent vector to the surface in the yz -plane with the same y -coordinate dy . Then the outward pointing surface element becomes $d\mathbf{S} = d\mathbf{s} \times d\boldsymbol{\ell} = (-dydz, dzdx, -dx dy)$ and thus

$$v_x dS_y - v_y dS_x = (v_x dx + v_y dy) dz = \mathbf{av} \cdot d\boldsymbol{\ell} dz.$$

This shows that the lift may be written as an integral over z

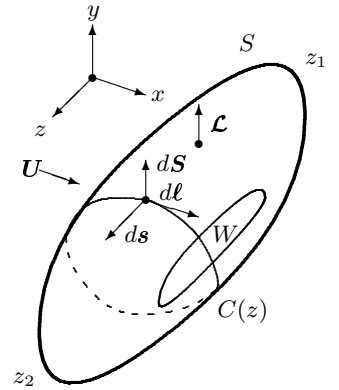
$$\mathcal{L} = \rho_0 U \int_{z_1}^{z_2} \Gamma(z) dz, \tag{27-37}$$

with an integrand that is the circulation around $C(z)$,

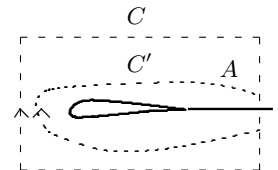
$$\Gamma(z) = \oint_{C(z)} \mathbf{v} \cdot d\boldsymbol{\ell}. \tag{27-38}$$

If the contour is deformed, Stokes’ theorem (16-67) tells us that the circulation is unchanged if the contour is swept through an area A devoid of vorticity. Since we have assumed that vorticity is only found in the boundary layers and the trailing wake, the contour may be freely deformed, as long as the piece of the contour that crosses the wake is kept fixed, and the new contour does not pass through the wake or into the boundary layers. This is of course the same conclusion as was reached in the preceding subsection.

Again it should be emphasized that no approximations have been made, and that this result is exactly valid, as long as the wake-crossing takes place at great distance from the body along a line parallel with the y -axis.



The surface S may always be sliced into a sequence of oriented planar curves $C(z)$ parallel with the xy -plane for $z_1 \leq z \leq z_2$.



The contours C and C' cross the trailing wake along the same curve (at infinity) and have the same circulation as long as the area A between the curves carries no flux of vorticity.

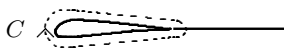
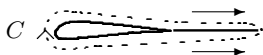
The Kutta-Joukowski theorem

The lift integral (27-37) may be written in the form of a generalized Kutta-Joukowski theorem (27-19),

$$\mathcal{L} = \rho_0 U L \langle \Gamma \rangle , \quad (27-39)$$

where

$$\langle \Gamma \rangle = \frac{1}{L} \int_{z_1}^{z_2} \Gamma(z) dz , \quad (27-40)$$



The dashed contour C hugs the wing profile closely, but is still attached to the distant part where it crosses the wake (top). For nearly infinite Reynolds number, the velocity is very nearly the same above and below the wake, allowing us to cut off the tail (bottom).

is the circulation along z averaged over the span $L = z_2 - z_1$. The only difference is that the integration contour $C(z)$ used to calculate $\Gamma(z)$ in (27-38) has to cross the wake far away from the airfoil, whereas in the original Kutta-Joukowski theorem it is supposed to hug the airfoil tightly all around. We shall now see how to get rid of the “tail” of the contour when the chordwise Reynolds number, $\text{Re}_c = Uc/\nu$ and the aspect ratio L/c are very large.

In this limit the flow around the wing becomes nearly ideal and irrotational, and the boundary layers turn into a “skin” of vorticity covering the airfoil with nearly vanishing thickness $\delta \sim 1/\sqrt{\text{Re}_c}$. Downstream from the airfoil, the skin continues into the trailing wake which forms a horizontal sheet, also of nearly vanishing thickness δ . Physically, the flow velocity in the wake cannot become infinite, so that the downstream volume flux in the wake, which per unit of span is of order $v_x \delta$, must itself vanish in the limit of infinite Reynolds number. It then follows from mass conservation that the orthogonal velocity v_y must be the same above and below the sheet, for otherwise fluid would flow into the sheet.

The pressure must also be the same above and below the trailing wake sheet because of Newton’s third law. Combining these two results with Bernoulli’s theorem, which states that $p + \frac{1}{2}\rho_0(v_x^2 + v_y^2 + v_z^2)$ takes the same value everywhere outside the wake, we conclude that $v_x^2 + v_z^2$ must be the same just above and below the wake. The span-wise induced flow v_z is connected to the shedding of vorticity along the span, especially the wing-tip vortices. When the aspect ratio is large, this flow will be tiny compared to the downstream flow, *i.e.* $|v_z| \sim v_x c/L \ll v_x$, so that it may be ignored in the Bernoulli function. Consequently, v_x itself takes the same value just above and below the trailing sheet. The two oppositely directed contributions to the integral (27-38) running along the tail of C thus tend to cancel each other for large Reynolds number and aspect ratio.

Since the orthogonal velocity v_y may not be infinite inside the wake, the part of the integral from the contour passing through the sheet will be of order of magnitude $v_y \delta$ and thus vanish in the limit. The contribution from the tail of the integration contour can thus be ignored in the leading approximation and we may let it circle the wing while hugging tightly to the airfoil profile all around. Finally, we have arrived at the (generalized) Kutta-Joukowski theorem.

Martin Wilhelm Kutta (1867–1944). *German mathematician. Probably best known for his extension of a method developed by Runge for numeric solutions to differential equations. Obtained the first analytic result for lift, and effectively discovered the relation between lift and circulation in 1902*

Nikolai Yegorovich Joukowski (1847–1921). *Russian mathematician and physicist (also spelled Zhukovskii). Constructed the first Russian wind tunnel in 1902 and many others early in the 20th century. Found and used the relation between lift and circulation in 1906*

* 27.7 Lift in two-dimensional airfoil theory

Most wings have fairly large aspect ratios in the vicinity of $L/c \approx 10 - 20$ with airfoil cross sections that taper gently towards the wing tips. For nearly infinite aspect ratio and nearly constant cross section, there is very little induced flow along z towards the wing tips, so that the flow becomes essentially two-dimensional,

$$\mathbf{v} = (v_x(x, y), v_y(x, y), 0) . \tag{27-41}$$

For such an airfoil, the circulation Γ is also independent of z .

The field of the vortex sheet

In the limit of nearly infinite Reynolds number, vorticity only exists in the infinitesimally thin boundary skins of the airfoil. Outside these skins and outside the infinitesimal sheet of the trailing wake, we assume that the flow is irrotational, described by a velocity potential Φ that satisfies Laplace's equation $\nabla^2\Phi = 0$. Being a linear equation, its solutions may be superposed. All the non-linearity of the original Euler equation has been collected in the Bernoulli pressure $p = \frac{1}{2}\rho_0(\mathbf{U}^2 - \mathbf{v}^2)$. The additivity of potential flows makes it possible to view the irrotational flow outside the boundary layers as arising from a superposition of the asymptotic flow \mathbf{U} and the field generated by the sheet of vorticity covering the wing surface.

Due to the two-dimensional nature of the flow, the vortex sheet making up the skin may be understood as a collection of elementary line vortex cores running parallel with the z -axis (see fig. 27.4). The velocity field from a line vortex passing through the origin of the coordinate system with the core parallel with the z -axis is of the well-known form (see section 23.1 on page 448)

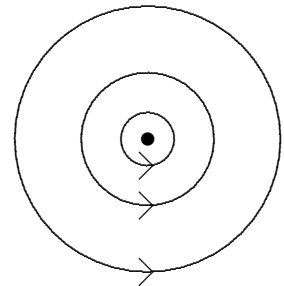
$$\mathbf{v} = \frac{\Gamma}{2\pi} \frac{(-y, x)}{x^2 + y^2} , \tag{27-42}$$

where Γ is its circulation or strength (counted positive clockwise in the xy -plane).

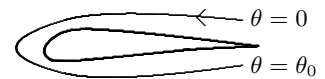
Denoting the infinitesimal strength of the vortex passing through the point (x', y') on the airfoil outline A by $d\Gamma'$, the complete velocity field becomes a curve integral around A ,

$$\mathbf{v}(x, y) = \mathbf{U} + \oint_A \frac{(-y + y', x - x')}{(x - x')^2 + (y - y')^2} \frac{d\Gamma'}{2\pi} . \tag{27-43}$$

Mathematically, the points of the airfoil outline should be parameterized as a pair of functions $(f_x(\theta), f_y(\theta))$ of a running parameter θ in some interval, say $0 \leq \theta \leq \theta_0$, beginning and ending at the cusp. Then $(x', y') = (f_x(\theta'), f_y(\theta'))$ and $d\Gamma' = \gamma(\theta') d\theta'$, where $\gamma(\theta')$ is the circulation density in θ' . We shall usually for clarity avoid this rather elaborate, though mathematically more concise, notation.



Outside the singular core of a line vortex the flow is irrotational with circular streamlines. The field around any collection of line vortices is obtained by adding their individual fields together.



The airfoil outline may be parameterized with a parameter θ running over the interval $0 \leq \theta \leq 2\pi$.

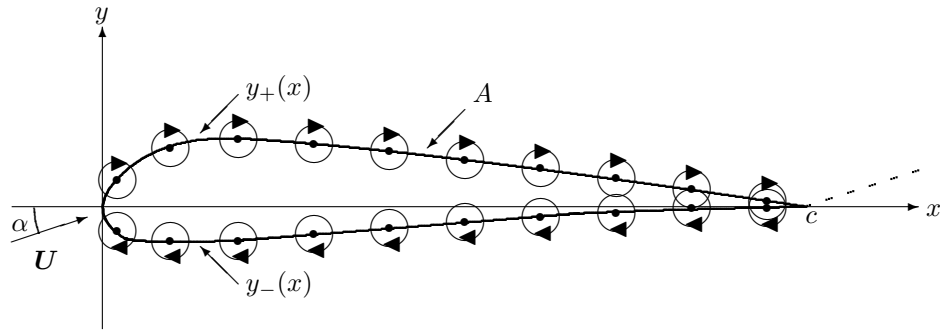


Figure 27.4: The irrotational field of the wing is viewed as a superposition of elementary line vortices with singular cores arranged around the outline A of the airfoil. On the top of the airfoil, the vortices tend to increase the velocity over the asymptotic flow \mathbf{U} , and conversely at the bottom. The airfoil is positioned with the chord-line on the x -axis and the y -axis at the leading edge. Its geometry is described by two functions $y_{\pm}(x)$ with $0 \leq x \leq c$ where c is the chord length. The asymptotic flow is $\mathbf{U} = U(\cos \alpha, \sin \alpha)$, where α is the angle of attack. The trailing wake, indicated by the dashed line, also forms an angle α with the x -axis. The z -axis comes out of the plane.

The Kutta condition

We may now contract the integration contour in (27-38) until it coincides with the airfoil outline A (fig. 27.4). Using that in ideal flow the velocity must be tangential to A , the circulation becomes

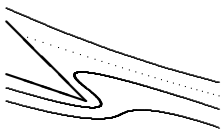
$$\Gamma = \oint_A \mathbf{v}(x, y) \cdot d\mathbf{l} = \oint_A |\mathbf{v}(x, y)| dl . \tag{27-44}$$

Locally each little line element dl of A contributes the infinitesimal amount,

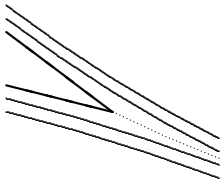
$$d\Gamma = |\mathbf{v}| dl \quad (\text{on } A) , \tag{27-45}$$

to the circulation.

Near the front and rear ends of the airfoil there are stagnation points where the velocity field vanishes. In ideal flow there may be more than one velocity field solution satisfying the Euler equation (16-1) and the boundary conditions. Such solutions may have different stagnation points and thus different circulation and lift. It is even possible to find a solution with vanishing circulation and lift. We shall see below that if the rear stagnation point is not situated right at the cusp of the trailing edge, unacceptable infinite velocity field values will arise at the cusp. The *Kutta condition* (1902) enforces that the trailing edge cusp (c in fig. 27.4) is actually a stagnation point. The condition thus repairs a mathematical problem in truly ideal flow by selecting a particular solution. In the real world, a streamlined airfoil with small angle of attack in nearly ideal flow will in fact fulfill the Kutta condition because of viscous friction in the boundary layers which selects a unique laminar solution.



Separating flow pattern near the trailing end of an airfoil with stagnation point before the cusp. Such a flow may have vanishing lift.

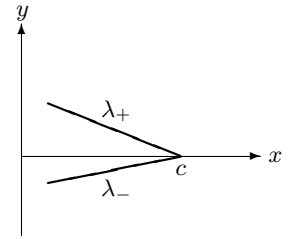


Highly laminar flow near the trailing end of an airfoil with stagnation point at the cusp.

In the neighborhood of the cusp the airfoil consists of two straight lines that may be parameterized by x , such that $y = \lambda_{\pm}(x - c)$ where λ_{\pm} are the (finite) slopes of the upper and lower halves of the airfoil outline. Denoting the corresponding circulation densities at the cusp by $d\Gamma/dx = \gamma_{\pm}$, and keeping only the two contributions to the integrand from the small interval $c - \epsilon < x' < c$, we find the divergent part of the velocity field

$$\mathbf{v}(c, 0) = \left[\frac{(\lambda_+, -1)\gamma_+}{1 + \lambda_+^2} + \frac{(\lambda_-, -1)\gamma_-}{1 + \lambda_-^2} \right] \int_{c-\epsilon}^c \frac{dx'}{x' - c} \quad (27-46)$$

The cusp field is evidently logarithmically divergent, unless $\gamma_+ = \gamma_- = 0$, *i.e.* unless the Kutta condition is fulfilled.



The cusp consists of two straight lines with different slopes $dy/dx = \lambda_{\pm}$.

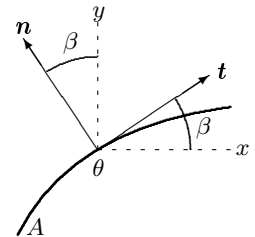
The fundamental airfoil equation

The circulation distribution $d\Gamma'$ must be chosen such that the streamlines follow the airfoil outline. This is equivalent to requiring the normal component of the velocity field to vanish on the impermeable airfoil surface, *i.e.*

$$\mathbf{v} \cdot \mathbf{n} = 0 \quad (\text{on } A) \quad , \quad (27-47)$$

where $\mathbf{v} = \mathbf{v}(x, y)$ is the velocity and $\mathbf{n} = \mathbf{n}(x, y)$ is the normal in the point (x, y) on A . For every point of A we thus get one scalar condition, and together with the Kutta condition that is sufficient to determine the vortex distribution $d\Gamma'$.

We are not at liberty to impose a no-slip condition on the field, because the Euler equation (16-1) is only of first order in the spatial derivatives. Although the field (27-43) exists both inside and outside the airfoil outline, the outside solution now fulfills the Euler equation and obeys the correct boundary conditions for inviscid flow around a solid body. Consequently, we may with impunity replace the region inside the airfoil outline with a solid body.



For convenience, the airfoil is positioned with its chord-line on the x -axis such that the asymptotic velocity becomes $\mathbf{U} = U(\cos \alpha, \sin \alpha)$ (see fig. 27.4). In the θ -parameterization, the tangent vector to the airfoil outline in the point θ is $\mathbf{t} = (\dot{x}, \dot{y}) = d(x, y)/d\theta$, where a dot denotes differentiation with respect to θ , and the normal may be taken to be $\mathbf{n} = (-\dot{y}, \dot{x})$. The boundary condition (27-47) now takes the explicit form

$$U(-\dot{x} \sin \alpha + \dot{y} \cos \alpha) = \oint_A \frac{\dot{x}(x - x') + \dot{y}(y - y')}{(x - x')^2 + (y - y')^2} \frac{d\Gamma'}{2\pi} \quad , \quad (27-48)$$

where now both $(x, y) = (f_x(\theta), f_y(\theta))$ and $(x', y') = (f_x(\theta'), f_y(\theta'))$ are points on A and $d\Gamma' = \gamma(\theta')d\theta'$.

Marvellously this equation can be integrated over θ . Using that for $\theta = 0$ we must have $x = c$ and $y = 0$, it may be verified by differentiation after θ that the following expression is the correct integral,

In any point $(x, y) = (f_x(\theta), f_y(\theta))$ of the airfoil outline, the tangent angle is denoted β and the slope $\lambda = \tan \beta = \dot{y}/\dot{x}$. The tangent vector may be chosen to be $\mathbf{t} = (\dot{x}, \dot{y})$ and the normal $\mathbf{n} = (-\dot{y}, \dot{x})$. The tangent angle β passes smoothly through 90° at the leading edge of the airfoil, whereas the slope passes through infinity.

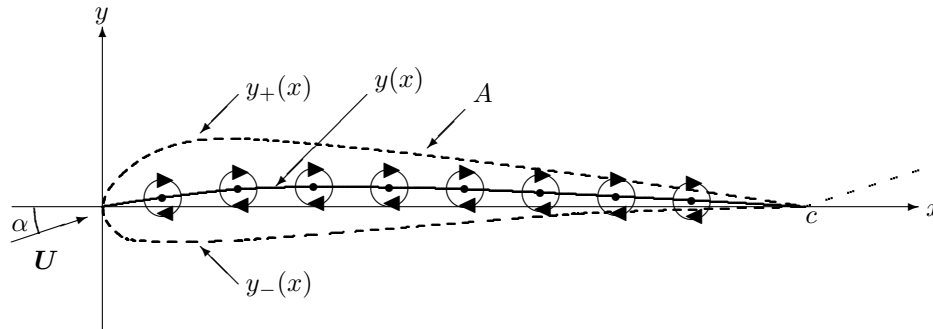


Figure 27.5: A thin airfoil is represented by a single layer of vorticity $\gamma(x) = \gamma_+(x) + \gamma_-(x)$ along the camber line $y(x) = \frac{1}{2}(y_+(x) + y_-(x))$.

$$U((c-x)\sin\alpha + y\cos\alpha) = \frac{1}{2} \oint_A \log \frac{(x-x')^2 + (y-y')^2}{(c-x')^2 + y'^2} \frac{d\Gamma'}{2\pi}. \quad (27-49)$$

This is the *fundamental equation of two-dimensional airfoil theory*. Given the parameterized airfoil geometry through the functions $(f_x(\theta), f_y(\theta))$, this integral equation should be solved for the vortex density $\gamma(\theta)$. Having done that, the total circulation Γ may afterwards be obtained by integrating the result,

$$\Gamma = \oint_A d\Gamma = \int_0^{\theta_0} \gamma(\theta) d\theta. \quad (27-50)$$

Finally, inserting this into the Kutta-Joukowski theorem (27-39), we obtain the lift. We have thus established a precise analytic or numeric procedure which for ideal flow will yield the lift as a function of the geometry of the airfoil.

Thin airfoil approximation

Even if modern airfoils are much thicker than the airfoils of the early airplanes, the ratio d/c of thickness to chord is rarely more than 10–15%. Using x as parameter, a decent approximation for thin airfoils is obtained by replacing the double layer of circulation density $\gamma_{\pm}(x)$ on the two halves of the airfoil outline by a single layer with $\gamma(x) = \gamma_+(x) + \gamma_-(x)$ distributed along the *camber line*,

$$y(x) = \frac{1}{2}(y_+(x) + y_-(x)). \quad (27-51)$$

For a thin airfoil with $d/c \ll 1$ we always have $|y(x) - y(x')| \ll |x - x'|$, so that the fundamental airfoil equation (27-49) degenerates into the much simpler

equation,

$$U((c-x)\sin\alpha + y(x)\cos\alpha) = \frac{1}{2\pi} \int_0^a \log \frac{|x-x'|}{c-x'} \gamma(x') dx' . \quad (27-52)$$

Given the camber line $y(x)$, this linear equation must be solved for $\gamma(x)$.

It is remarkable that we can obtain the circulation directly by means of the strange integral,

$$\int_0^c \frac{c}{(c-x)\sqrt{x(c-x)}} \log \frac{|x-x'|}{c-x'} dx = -2\pi , \quad (27-53)$$

which is true for all $c > 0$ and all x' between 0 and c . It takes a fair bit of complex analysis to prove this (see problem 27.6), but it may easily be checked numerically. Using this result in (27-52) we get the circulation

$$\Gamma = \int_0^c \gamma(x') dx' = -cU \int_0^c \frac{(c-x)\sin\alpha + y(x)\cos\alpha}{(c-x)\sqrt{x(c-x)}} dx . \quad (27-54)$$

Using that $\int_0^c dx/\sqrt{x(c-x)} = \pi$, the first part of the integral is trivial, and we finally get

$$\Gamma = -Uc \left(\pi \sin\alpha + \cos\alpha \int_0^c \frac{y(x)}{(c-x)\sqrt{x(c-x)}} dx \right) . \quad (27-55)$$

The integral converges because $y(x) \sim c-x$ for $x \rightarrow c$.

Taking into account that the contour of integration in the Kutta-Joukowski theorem (27-39) is clockwise and not counterclockwise as assumed in the above calculation, the lift is $\mathcal{L} = -\rho_0 U L \Gamma$. For small angles of attack, $|\alpha| \ll 1$, the lift coefficient takes the form (27-22),

$$C_L = \frac{\mathcal{L}}{\frac{1}{2}\rho_0 U c L} = 2\pi(\alpha - \alpha_0) , \quad (27-56)$$

with zero lift angle,

$$\alpha_0 = -\frac{1}{\pi} \int_0^c \frac{y(x)}{(c-x)\sqrt{x(c-x)}} dx . \quad (27-57)$$

Since airfoils have mostly positive camber, $y(x) > 0$, it follows that $\alpha_0 < 0$. For a flat plate we evidently have $\alpha_0 = 0$ because $y(x) = 0$.

* 27.8 The distant laminar wake

At short distances the velocity field is strongly dependent on the shape and attitude of a moving body, but far from the body such details are lost. It is, as we shall now see, possible to determine the general form of the laminar velocity field at large distances from the body in terms of the lift and drag that the body produces (see also [57, p. 67]). The analysis in this section should be viewed as the natural continuation of d'Alembert's theorem to fluids that are not perfectly inviscid. Such fluids will not "close up" behind the moving body, but instead — as we have discussed above — leave a trailing wake, a disturbance that never dies completely out even at huge distance behind the body. In the real unruly and turbulent atmosphere, the trailing wake from a passing airplane will of course only be noticeable for a finite distance.

Oseen's approximation

Sufficiently far from the body, the velocity field is laminar and approximatively equal to the asymptotic value \mathbf{U} both inside and outside the trailing wake. Inserting $\mathbf{v} = \mathbf{U} + \Delta\mathbf{v}$ into the steady flow equation,

$$(\mathbf{v} \cdot \nabla)\mathbf{v} = -\frac{1}{\rho_0}\nabla p + \nu\nabla^2\mathbf{v} , \quad (27-58)$$

we obtain to first order in $\Delta\mathbf{v}$,

$$(\mathbf{U} \cdot \nabla)\Delta\mathbf{v} = -\frac{1}{\rho_0}\nabla p + \nu\nabla^2\Delta\mathbf{v} . \quad (27-59)$$

The linearity of this equation allows us to superpose its solutions. Let us write the velocity difference as a sum,

$$\Delta\mathbf{v} = \mathbf{u} + \nabla\Phi , \quad (27-60)$$

where Φ is a generalized velocity potential chosen as a solution to

$$(\mathbf{U} \cdot \nabla)\Phi = -\frac{p}{\rho_0} + \nu\nabla^2\Phi . \quad (27-61)$$

Using this to eliminate p in (27-59), it follows that the field \mathbf{u} must satisfy

$$\boxed{(\mathbf{U} \cdot \nabla)\mathbf{u} = \nu\nabla^2\mathbf{u}} . \quad (27-62)$$

The incompressibility condition, $\nabla \cdot \Delta\mathbf{v} = 0$, yields a relation between Φ and \mathbf{u}

$$\boxed{\nabla^2\Phi = -\nabla \cdot \mathbf{u}} . \quad (27-63)$$

The system of equations now closes in a simple way: If \mathbf{u} is a solution to (27-62), this equation determines Φ , and then from (27-61) the pressure may be obtained.

Flow inside the wake

The trailing wake is assumed to be narrow compared to the distance to the body. In a coordinate system with the x -axis along the asymptotic velocity, $\mathbf{U} = U\mathbf{e}_x$, we may assume that $x \gg |y|, |z|$, inside the wake. In the now familiar way, it follows that the double x -derivative in the Laplacian of (27-62) is small compared with the y, z -derivatives, and the equation for \mathbf{u} becomes

$$U \frac{\partial \mathbf{u}}{\partial x} = \nu \left(\frac{\partial^2}{\partial y^2} + \frac{\partial^2}{\partial z^2} \right) \mathbf{u} . \quad (27-64)$$

This is a standard diffusion equation of the same form as the momentum diffusion equation (18-5) with two transverse dimensions and “time” $t = x/U$. Notice that this is also the time, it takes for the asymptotic flow to reach the downstream position x from the body.

At distances much larger than the body size, $x \gg L$, the body appears as a point particle with no discernable shape, situated at the origin of the coordinate system. By insertion into the above equation one may verify that the following expression is an exact “shapeless” solution,

$$\mathbf{u} = \frac{\mathbf{A}}{x} \exp \left(-U \frac{y^2 + z^2}{4\nu x} \right) , \quad (27-65)$$

where $\mathbf{A} = (A_x, A_y, A_z)$ is a constant vector. It is in fact also the most general solution at large downstream distance x (see problem 27.8). Evidently, the distant wake has a Gaussian shape in the transverse directions with a narrow width $\delta = \sqrt{4\nu x/U}$. The width of the laminar wake is, however, the same in both transverse directions, confirming that there is no imprint of the original shape of the object on the Gaussian form of the distant wake. Taking $y, z \sim \sqrt{x}$, the solution decays as x^{-1} along the wake, rather than the expected $r^{-2} \approx x^{-2}$. This is consistent with the area of the wake being of order $\delta^2 \sim x$ such that the integral of \mathbf{u} over the cross section of the wake remains finite for $x \rightarrow \infty$. The terms that have been left out in the above solution by dropping the x -derivatives in the Laplacian are a further factor x^{-1} smaller than the above solution and cannot contribute in the limit.

The generalized potential is determined by solving (27-63). Consistently leaving out the double derivatives in the Laplacian, it becomes

$$\left(\frac{\partial^2}{\partial y^2} + \frac{\partial^2}{\partial z^2} \right) \Phi = -\nabla \cdot \mathbf{u} . \quad (27-66)$$

On the right hand side one cannot leave out the $\nabla_x u_x$ contribution to the divergence because it is only a factor $x^{-1/2}$ smaller than the others. It may — with some effort — be verified by insertion that the following potential is an exact solution to this equation

$$\Phi = \frac{2\nu}{U} \left(-\frac{A_y y + A_z z}{y^2 + z^2} + \frac{A_x}{2x} \right) \left(1 - \exp \left(-U \frac{y^2 + z^2}{4\nu x} \right) \right) . \quad (27-67)$$

Here the first term in the first parenthesis is of order $x^{-1/2}$ and the second of order x^{-1} . The leading corrections from leaving out the double derivatives in the Laplacian are of order $x^{-3/2}$. Only the exponential in the second parenthesis represents a true solution to the inhomogeneous equation (27-66), to which one may add an arbitrary solution to Laplace's equation $\nabla^2\Phi = 0$. Here we have added the solution which makes the potential regular for $y = z = 0$.

Drag and lift

The pressure is obtained in the same approximation from (27-61),

$$p = -\rho_0 U \frac{\partial\Phi}{\partial x} + \rho_0 \nu \left(\frac{\partial^2}{\partial y^2} + \frac{\partial^2}{\partial z^2} \right) \Phi = \rho_0 \nu \frac{A_x}{x^2} . \quad (27-68)$$

Since it decays like x^{-2} and the area of the wake is $\delta^2 \sim x$, it cannot contribute to drag for $x \rightarrow \infty$, so that the leading contribution to the integrand of (27-33) becomes

$$p + \rho_0 U \Delta v_x \approx \rho_0 U u_x . \quad (27-69)$$

In the last step we have dropped the pressure and the potential derivative $\nabla_x \Phi \sim x^{-3/2}$ which are both negligible compared to $u_x \sim x^{-1}$. Integrating over all y, z , we find from (27-33)

$$\mathcal{D} \approx -\rho_0 U \iint u_x \, dydz = -4\pi\rho_0\nu A_x . \quad (27-70)$$

which fixes the coefficient A_x . The errors committed in extending the integral over the wake to all values of y and z are exponentially small.

The lift is obtained from the complete circulation integral (27-38),

$$\Gamma(z) = \oint_{C(z)} (\mathbf{u} + \nabla\Phi) \cdot d\boldsymbol{\ell} = \oint_{C(z)} \mathbf{u} \cdot d\boldsymbol{\ell} \approx - \int u_y dy .$$

In the second step we have used that Φ is single-valued so that $\oint \nabla\Phi \cdot d\boldsymbol{\ell} = 0$, and in the third that \mathbf{u} vanishes outside the wake slice, $W(z)$. The minus sign stems from the contour running through the wake against the direction of the y -axis. Inserting this result into (27-37) we find

$$\mathcal{L} = -\rho_0 U \iint u_y \, dydz = -4\pi\nu\rho_0 A_y , \quad (27-71)$$

which fixes A_y . Similarly, since there is no lift in the z -direction, we must have $A_z = 0$.

The complete field configuration inside the wake has now been obtained in terms of the lift and drag that the body generates,

$$\begin{aligned} \mathbf{u} &= -\frac{(\mathcal{D}, \mathcal{L}, 0)}{4\pi\rho_0\nu x} \exp\left(-U\frac{y^2+z^2}{4\nu x}\right), \\ \Phi &= \frac{1}{4\pi\rho_0 U x} \left(\frac{2xy}{y^2+z^2}\mathcal{L} - \mathcal{D}\right) \left(1 - \exp\left(-U\frac{y^2+z^2}{4\nu x}\right)\right). \end{aligned} \quad (27-72)$$

The correction terms are all of *relative* order x^{-1} .

Flow outside the wake

Outside the wake, the flow is assumed to be irrotational with $\Delta\mathbf{v} = \nabla\Phi$ and $\nabla^2\Phi = 0$. We have before argued that $\Delta\mathbf{v} \sim 1/r^2$ at large distances, and consequently we must have $\Phi \sim 1/r$. In spherical coordinates with the polar axis in the x -direction and the null-meridian in the xy -plane, we may thus write

$$\Phi = \frac{F(\theta, \phi)}{r}. \quad (27-73)$$

The spherical Laplacian (C-16) implies that F has to satisfy

$$\left(\sin^2\theta\frac{\partial^2}{\partial\theta^2} + \cos\theta\sin\theta\frac{\partial}{\partial\theta} + \frac{\partial^2}{\partial\phi^2}\right)F = 0. \quad (27-74)$$

In view of the periodicity in ϕ , the complete solution may be written as a Fourier series

$$F = A_0(\theta) + \sum_{n=1}^{\infty} A_n(\theta) \cos n\phi + B_n(\theta) \sin n\phi, \quad (27-75)$$

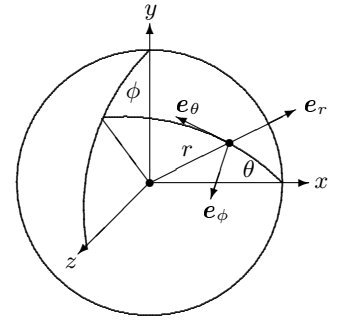
where the coefficients A_n and B_n satisfy the equation

$$\left(\sin^2\theta\frac{d^2}{d\theta^2} + \cos\theta\sin\theta\frac{d}{d\theta} - n^2\right)A_n = 0. \quad (27-76)$$

Surprisingly, this equation has the exact solutions $(\tan\frac{\theta}{2})^{\pm n}$ (see problem 27.9). Since F has to be regular at $\theta = \pi$, only the negative sign is acceptable. Furthermore, for $\theta \rightarrow 0$, where $A_n \sim \theta^{-n}$, this solution has to join continuously with the inside solution (27-72), which for $y, z \gg \delta$ and $y, z \ll x$ behaves like

$$\Phi \approx \frac{1}{4\pi\rho_0 U x} \left(\frac{2xy}{y^2+z^2}\mathcal{L} - \mathcal{D}\right) \approx \frac{\mathcal{L}}{2\pi\rho_0 U} \frac{\cos\phi}{r\theta} - \frac{\mathcal{D}}{4\pi\rho_0 U r}. \quad (27-77)$$

This shows that the only possible exponents are $n = 0, 1$ with $A_0 = -\mathcal{D}/4\pi\rho_0 U$, $A_1 = \mathcal{L}/4\pi\rho_0 U$ and $B_1 = 0$. Thus the potential far from the body outside the



Spherical coordinates and their tangent vectors for the far field outside the wake.

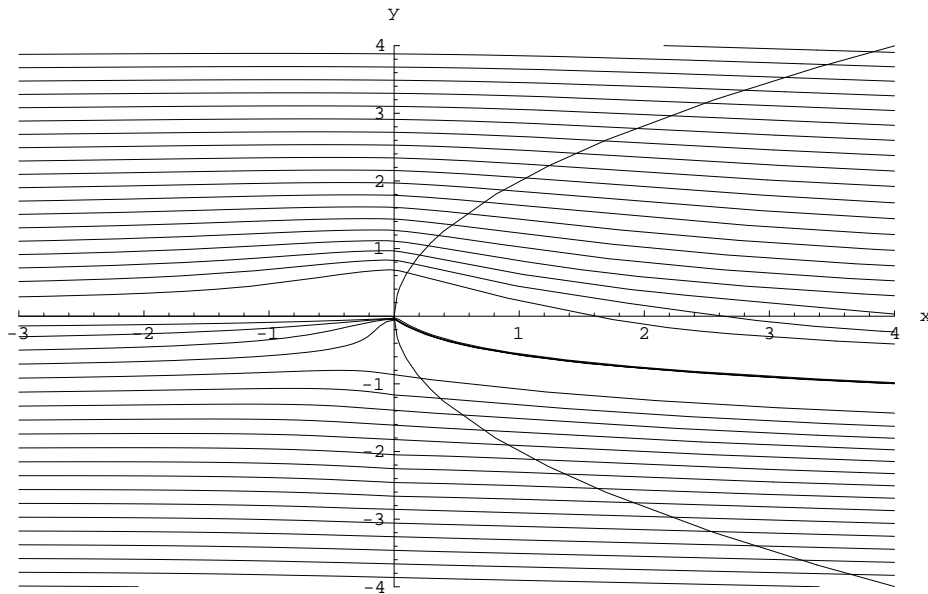


Figure 27.6: Streamlines for the far field in the $z = 0$ plane. The parameters for the plot are $U = \rho_0 = \nu = 1$, $\mathcal{D} = 5$, and $\mathcal{L} = 10$. The parabola defines the width of the laminar wake, $y = 2\sqrt{\nu x/U}$. The far field has been regulated such that it is well-defined and finite everywhere (see problem 27.10). The regulated flow violates the compressibility condition $\nabla \cdot \mathbf{v} = 0$ near the center. The gap is an artefact of the regulation, which makes the “body” appear to have a funnel at the center, making some the streamlines converge behind the body. Notice the downwards flow behind the body, caused by the lift.

wake becomes

$$\Phi = \frac{\mathcal{L} \cos \phi \cot(\theta/2) - \mathcal{D}}{4\pi\rho_0 U r}. \quad (27-78)$$

It joins continuously with the field of the wake. The streamlines for the combined inside and outside fields are shown in fig. 27.6 in a convenient interpolating approximation (see problem 27.10).

Pressure and lift

Since the leading contribution to pressure vanishes far downstream inside the wake, it plays no role for the drag which as shown by (27-70) is entirely due to a loss of fluid momentum. The lift contribution from pressure similarly stems entirely from the outside solution. Using Bernoulli’s theorem and the spherical derivatives (C-14), the outside pressure becomes, $p = -\rho_0 U \nabla_x \Phi = -\rho_0 U (\cos \theta \nabla_r - \sin \theta \nabla_\theta) \Phi$. After a bit of algebra this reduces to,

$$p = -\frac{\mathcal{D} + \mathcal{L} \sin \theta \cos \phi}{4\pi r^2}. \quad (27-79)$$

It is immediately clear that the spherically symmetric first term cannot contribute to the total contact force. Also since $dS_x = \cos \theta \cdot r^2 \sin \theta d\theta d\phi$, the second term which is linear in $\cos \phi$ cannot produce a force in the x -direction, *i.e.* a drag.

Due to its ϕ -dependence the second term is, however, negative above the xz -plane and positive below, and must therefore produce a lift. Using that $dS_y = \sin \theta \cos \phi \cdot r^2 \sin \theta d\theta d\phi$, we find

$$-\oint p dS_y = \frac{\mathcal{L}}{4\pi} \iint \sin^3 \theta \cos^2 \phi d\theta d\phi = \frac{1}{3} \mathcal{L} . \quad (27-80)$$

Pressure thus produces one third of the lift, even for an infinite sphere. The remaining two thirds of lift stems from momentum flux. As discussed before (page 557), the partition of lift between pressure and momentum flux depends on the choice of integration surface at infinity. The pressure contribution would vanish if the “box” at infinity were taken to be a huge cylinder with length much smaller than radius.

Problems

27.1 The Concorde airliner has a powerplant of four engines that together develop 677 kN with afterburner. Its maximal takeoff mass is 185,000 kg and its takeoff speed 360 km/h. Ignore drag and calculate the runway a) acceleration, b) time and c) length.

27.2 Show that the tangent to the bank angle in a horizontal banked turn is 2π times the ratio between the time it takes to fall freely from rest to velocity U (with no air resistance) divided by the time T it takes to make a complete turn.

27.3 Show that the induced drag is smaller if the single trailing vortex is divided into a number of smaller vortices coming off the wing.

27.4 Let $e_U = \mathbf{U}/U$ be a unit vector in the direction of the asymptotic flow. a) Show that the drag is always of the form

$$\mathcal{D} = \oint_S (p + \rho_0 \Delta \mathbf{v} \cdot \mathbf{U}) \mathbf{e}_U \cdot d\mathbf{S} , \quad (27-81)$$

and that the lift takes the form

$$\mathcal{L} = -\rho_0 \oint_S \mathbf{U} \times (\Delta \mathbf{v} \times d\mathbf{S}) + \oint_S p \mathbf{e}_U \times (\mathbf{e}_U \times d\mathbf{S}) . \quad (27-82)$$

b) Show that the last term vanishes if S cuts the wake in a planar region orthogonal to the asymptotic velocity.

* **27.5** Show explicitly that the sheet vortex field (27-43) has circulation

$$\Gamma = \oint_C \mathbf{v} \cdot d\boldsymbol{\ell} = \oint_A d\Gamma \quad (27-83)$$

where C is an arbitrary curve completely surrounding the airfoil A .

* **27.6** Show that

$$\int_0^1 \frac{1}{(1-t)\sqrt{t(1-t)}} \log \frac{|t-x|}{1-x} dt = -2\pi , \quad (27-84)$$

for all x .

* **27.7** Assume that a thin airfoil has camber function

$$\Delta y(x) = k \sqrt{\frac{x}{a}} (a-x) \quad (27-85)$$

where $k \ll 1$. Calculate the zero-lift angle α_0 .

* **27.8** Consider the N -dimensional diffusion equation in the variables $x = (x_1, \dots, x_N)$

$$\frac{\partial F}{\partial t} = \sum_{n=1}^N \frac{\partial^2 F}{\partial x_n^2} \quad (27-86)$$

(a) Show that with initial data $F(x, 0) = F_0(x)$, the solution at time t is

$$F(x, t) = (4\pi t)^{-N/2} \int F_0(y) \exp\left(-\frac{(x-y)^2}{4t}\right) d^N y \quad (27-87)$$

where $(x-y)^2 = \sum_n (x_n - y_n)^2$.

(b) Show that if $F_0(y)$ is bounded or decreases at least as rapidly as a Gaussian for $|y| \rightarrow \infty$, the the solution for $t \rightarrow \infty$ is

$$F(x, y) = (4\pi t)^{-N/2} \exp\left(-\frac{x^2}{4t}\right) \int F_0(y) d^N y \quad (27-88)$$

* **27.9** Find all solutions to

$$\left(\sin^2 \theta \frac{d^2}{d\theta^2} + \cos \theta \sin \theta \frac{d}{d\theta} - n^2\right) f = 0 . \quad (27-89)$$

* **27.10** The streamline plot of fig. 27.6 is from the following field,

$$v_x = U + u_x + \nabla_x \Phi , \quad (27-90)$$

$$v_y = u_y + \nabla_y \Phi , \quad (27-91)$$

$$v_z = \nabla_z \Phi \quad (27-92)$$

where

$$u_x = -\frac{\mathcal{D}}{4\pi\rho_0\nu(a+r)}W \quad (27-93)$$

$$u_y = -\frac{\mathcal{L}}{4\pi\rho_0\nu r}W , \quad (27-94)$$

$$\Phi = \frac{1}{4\pi\rho_0U r} \left(\mathcal{L} \frac{(r+x)y}{b^2 + y^2 + z^2} - \mathcal{D} \right) (1 - W) . \quad (27-95)$$

where $r = \sqrt{x^2 + y^2 + z^2}$, and W is the “wake-factor”

$$W = \exp\left(-U \frac{y^2 + z^2}{4\nu(a+x)}\right) \theta(x) . \quad (27-96)$$

Here $\theta(x) = 1$ for $x > 0$ and 0 for $x < 0$, and a and b are positive constants, in the figure chosen to be $a = 1$ and $b = 0.3$.

Show that this field is defined all over space and that it approximates the far field at great distances both inside and outside the wake.

